

# Cyclonic Eddies and Upper-Thermocline Finescale Structures in the Antarctic Circumpolar Current

Harry Leach<sup>\*†</sup> & Volker Strass<sup>‡</sup>

Thursday 29<sup>th</sup> November, 2018

## Abstract

Mesoscale eddies in the open ocean are mostly formed by baroclinic instability, in which the available potential energy from the large scale slope of the isopycnals is converted into the kinetic energy of the flow around the eddy. As a permissible form of motion within a rapidly rotating and stratified fluid eddies driven by baroclinic instability are important for the poleward and vertical transport, not only of physical properties, but also biogeochemical ones.

In this paper we present observations from four cyclonic eddies in the Antarctic Circumpolar Current. We have sorted them by apparent age, based on altimeter data and consideration of the degree of homogenisation of the potential temperature-salinity( $\theta S$ )-relationship, and then looked at the spatial distribution of measures of finescale variability in the upper thermocline.

The youngest eddy shows isopycnals which are domed upwards and it contains a variety of waters with differing temperature-salinity characteristics. The finescale variability is higher in the core of the eddy. The older eddies show a core which is more homogeneous in potential temperature and salinity. The isopycnals are flatter in the centre of the eddy and in cross-section they can be M-shaped, so that the steepest gradients are concentrated around the edge. The finescale variability is more concentrated around the edges where the density gradients are stronger.

We hypothesise that lateral stirring and mixing processes within the eddy homogenise the water so that the temperature-salinity relationship becomes tighter. When the eddy eventually collapses this modified water can be released back into the flow. Thus we see how the interplay of mesoscale and small scale processes are modifying water mass properties and, potentially, regulate biogeochemical processes.

---

\*Corresponding Author, <http://orcid.org/0000-0003-1774-5167>

<sup>†</sup>Department of Earth, Ocean and Ecological Sciences, University of Liverpool, 4 Brownlow Street, Liverpool, L69 3GP, UK. Email: leach@liv.ac.uk, Tel +44 151 794 4097

<sup>‡</sup>Alfred-Wegener-Institut, Helmholtz-Zentrum für Polar- und Meeresforschung, Postfach 12 01 61, D-27515 Bremerhaven, Germany.

# 1 Introduction

Mesoscale eddies in the open ocean are generally formed by baroclinic instability, in which the available potential energy from the large scale slope of the isopycnals is converted into the kinetic energy of the flow around the eddy. Work on eddies began in the atmosphere with theories of baroclinic instability being evolved in the 1940s (Charney, 1947; Eady, 1949) to explain synoptic scale weather systems. At this time oceanographers were more concerned with understanding the basin-scale wind-driven gyres (Sverdrup, 1947; Stommel, 1948; Munk, 1950). When, however, oceanographers tried to observe this slow, steady, large basin-scale flow ( $\sim \text{cm s}^{-1}$ ) they found that it was masked by much stronger variable flow ( $\sim 10\text{s cm s}^{-1}$ ) on smaller scales, 10s to 100s km. This led to the Mid-Ocean Dynamics Experiment 1973 (MODE 1978) and the realisation that baroclinic instability was also important in the ocean (Gill et al., 1974).

The initial instability theories were only concerned with the exponential growth of a small disturbance, but then attention turned to eddy life cycles. Edmon et al. (1980) described how, as a baroclinic disturbance grows, heat is transported polewards and the available potential energy of the mean flow is converted to eddy kinetic energy. However, after passing maturity, the eddy decays and momentum is fed back *into* the jet and eddy kinetic energy returns to the kinetic energy of the mean flow. Work on the way in which eddies decay was done by Methven (1998) and Methven and Hoskins (1998, 1999); their calculations showed that, as an eddy forms, it winds in anomalies of potential vorticity, which eventually leads to an unstable situation and the eddy collapses releasing anomalies back into the mean flow. The interesting point is that once formed eddies do not simply decay by friction running them down, but rather collapse quickly. Chelton et al. (2011) have looked at the statistical properties of eddies based on the AVISO altimeter data and show that about 10% last 16 weeks or more, which corresponds to a half-life of about 5 weeks.

One of the processes which contribute to the evolution of eddies are finescale interleavings; these are thermohaline anomalies with a vertical scale of tens of metres, arising due to ageostrophic flow across fronts as part of the frontogenesis process (Joyce 1977, MacVean and Woods 1980, Woods et al. 1986). Frontogenesis is itself a process by which density and thermohaline gradients can sharpen on scales smaller than that of the eddies.

The Antarctic Circumpolar Current (ACC) is one of the most eddy-rich regions of the ocean; here the eddy transports across the ACC are particularly important for the global meridional overturning (Marshall and Speer, 2012) and the subduction of anthropogenic  $\text{CO}_2$  (Sallée et al. 2012, Bopp et al. 2015). Drake Passage, as one of the more accessible parts of the ACC, has received particular attention. Joyce et al. (1978) looked at the character of the interleavings near the Antarctic Polar Front (APF) and more recently Thompson et al. (2007) looked at vertical diffusion on either side of the APF and reported that it is higher to the north than to the south. Earlier work on the genesis of cyclonic eddies from the APF in Drake Passage (Joyce et al. 1981, Peterson et al. 1982) largely focussed on the bulk properties, such as heat and freshwater content anomalies, as indeed have more recent studies (Swart et al. 2008, Kurczyn et al. 2013, Zhang et

71 al. 2016). However, Joyce et al. (1981) do present a CTD section through a cyclonic  
72 eddy apparently freshly formed during the course of their experiment from the APF and  
73 it appears to display greater interleaving on the edges. Adams et al. (2017) present  
74 sections from a towed system crossing the rim of a freshly formed cyclonic eddy in the  
75 Scotia Sea. The most complicated submesoscale structures are observed in the saddle  
76 region where the eddy is separating from its parent front. However, their sections do not  
77 extend to the centre of the eddy.

78

79 Armi and Zenk (1984) present a detailed study of lenses of high salinity water which were  
80 formed in the Mediterranean Outflow and then propagate southwestwards in the Canaries  
81 Basin. These "Meddies" are anticyclonic and have ages which may be measured in years,  
82 rather than months, and they too show stronger finescale variability around the edges  
83 than in the centre (Meunier et al. 2015). More generally in recent years sub-mesoscale co-  
84 herent vortices (SCV), first named by McWilliams (1985), have attracted much interest.  
85 These are generally anticyclonic sub-surface features so that, in the northern hemisphere,  
86 they can have very negative relative vorticity, so that their Ertel potential vorticity can  
87 be negative. It seems that they are often generated by the interaction of boundary cur-  
88 rents with topography (D'Asaro 1988, Molemaker et al. 2015, Thomsen et al. 2016).  
89 Pietri and Karstensen (2018) describe the anatomy of a seven-month old SCV formed  
90 near the coast of Mauretania and show that there is enhanced interleaving around the rim.

91

92 In this study data from four eddies, or mesoscale features, were used, all from the Atlantic  
93 sector of the ACC. The ACC consists of a series of fronts (Gordon 1971, Gordon et al.  
94 1977, Orsi et al. 1995, Sokolov and Rintoul 2009), or jets, which can become unstable  
95 and form eddies. All four cyclonic features studied contained lenses of cold Winter Water  
96 (WW) with temperature minima in the depth range 100-300 m and were trapped in the  
97 zone between the Antarctic Polar Front and the Southern Polar Front (Hibbert et al.  
98 2009, Strass et al. 2017a). Close inspection of the character and structure of these four  
99 eddies combined with estimates of their ages from altimeter data suggests how eddies  
100 might evolve after they have formed. In this paper we will consider both the mesoscale  
101 structure of the eddies, in terms of maps, sections and  $\theta S$  diagrams, and also the distribu-  
102 tion of measures of fine scale variability. By looking at both the mesoscale and fine scale  
103 properties of the eddies we can gain some insight into how the properties of water masses  
104 trapped in eddies might be modified before rerelease into the general flow. It should be  
105 stressed though, that, while we have used parameters derived from individual CTD pro-  
106 files as measures of finescale variability, we are nevertheless of the opinion that, so far as  
107 the mesoscale is concerned, lateral stirring by sub-mesoscale processes and then mixing  
108 are more important than diapycnic processes alone (see Hibbert et al. 2009, Smith and  
109 Ferrari 2009, Leach et al. 2011).

110

111 In addition to controlling the exchange of physical properties across the ACC eddies are  
112 involved in the interplay of physical, chemical and biological processes which limit pri-  
113 mary productivity, and hence CO<sub>2</sub> drawdown, in the Southern Ocean. The supply of  
114 silica or iron, limitation by light and grazing pressure are all held to be contributory  
115 factors by a variety of authors (see for example Martin 1990, Moore and Abbott 2000,  
116 2002, Ito et al. 2005, Behrenfeld 2010, Hoppe et al. 2017) but the horizontal and vertical

117 rates of exchange will be controlled by the eddy field (Strass et al. 2002, Jones et al. 2017).

118

119 This study is largely based on data obtained by vertical CTD casts; although other data  
120 were collected during some of the surveys, it was by no means so systematic and uni-  
121 form as the basic CTD cast data. Vessel-mounted ADCP data are available for all the  
122 surveys and shown in Hibbert et al. (2009) and Strass et al. (2017a), but generally just  
123 show the same eddy structure as the hydrography and so have not been repeated here.  
124 This study makes use of a variety of parameters from the upper thermocline, starting  
125 below the surface layer at 100 m depth and extending to the potential temperature max-  
126 imum of the Upper Circumpolar Deep water at about 500 m depth and encompassing  
127 the Winter Water potential temperature minimum at about 150 m depth. At the low  
128 temperatures in question the non-linearity of the equation of state means that density  
129 depends almost solely on salinity, so that temperature can be regarded as a passive tracer.

130

131 In this paper we have adopted the convention that the units of temperature (relative  
132 to the freezing point of pure water) are °C while units of temperature difference are K.  
133 At the low temperatures encountered temperatures and temperature differences can be  
134 numerically similar and this convention helps distinguish between them.

## 135 2 Data

136 Both the cruises, from which the data were used in this study, were primarily biogeochem-  
137 ical in their aims, designed to study either artificially stimulated or naturally occurring  
138 phytoplankton blooms so that the work reported here is essentially a by-product using  
139 data not designed for the purpose.

140

141 The track of *Polarstern* Cruise ANTXXI/3 – "EIFEX" – leaving from Cape Town on  
142 21st January 2004 (Smetacek, 2005) and arriving back in Cape Town on 25th March  
143 2004 is shown in Figure 1. The purpose of this cruise was to conduct an iron fertilisation  
144 experiment in the ACC. The reason for using an eddy was that the water fertilised with  
145 iron sulphate would be trapped and relatively easy to follow (Strass et al. 2005). The first  
146 eddy (Eddy 1) selected on the basis of altimeter data was at about 50°S, 18°E. This eddy  
147 was surveyed during a period of 7 days between 25th January and 1st February 2004 by  
148 CTD/Rosette casts along 5 equally spaced meridional sections. Along the westernmost  
149 section, 17°E, the station spacing was 5 miles (9 km) and along the other four (17°40',  
150 18°20', 19°00' and 19°40'E) it was 12 miles (22 km); the sections were completed sys-  
151 tematically working from west to east. Investigation revealed that the initial chlorophyll  
152 concentration was too low for the fertilisation experiment and so this eddy was rejected,  
153 but not before a useful set of physical data had been obtained. Instead, a second eddy  
154 (Eddy 2), at about 49°S, 2°E was selected for the experiment and was ultimately occu-  
155 pied for a period of 40 days. Altogether this eddy was investigated during the period  
156 8th February to 20th March 2004, however the data for the initial CTD/Rosette survey  
157 were collected during a period of 6 days between 14th and 20th February; the stations  
158 were evenly spaced 12 miles (22 km) apart meridionally and zonally, or 12' latitude and  
159 about 18.6' of longitude, with ten stations along each of eight equally spaced meridional

160 sections between 1°19' and 3°29'E. The sections were collected systematically from west  
161 to east. This second eddy was the one from which Smetacek et al. (2012) reported on  
162 the massive export event at the end of the iron-fertilised bloom. Hibbert et al. (2009)  
163 used the evolution of the core temperature of this eddy to draw conclusions about the  
164 rate of mixing of water within the eddy and compared the  $\theta$ S relationships to support  
165 their ideas about the homogenisation of properties within the eddy over time.

166  
167 The track of *Polarstern* Cruise ANTXXVIII/3 – "Eddy-Pump" – leaving from Cape Town  
168 on 7th January 2012 and arriving in Punta Arenas on 11th March 2012 (Wolf-Gladrow,  
169 2013) is shown in Figure 2. The purpose of this cruise was to look at naturally-occurring  
170 late-season phytoplankton blooms in the ACC; most of the biogeochemical results of this  
171 cruise are published in Strass et al. (2017b). Unusually, this time the Atlantic Sector  
172 of the Southern Ocean seemed devoid of any useful isolated eddies, so that initially a  
173 meridional section across the ACC was made at 10°E. After that two mesoscale features  
174 were investigated. The first was on the west side of the Mid-Atlantic Ridge at about 51°S,  
175 13°W (the West Mid-Atlantic Ridge Survey, WMAR) and the second was in the Georgia  
176 Basin at about 50°S, 38°W (the Georgia Basin Survey, GeoB). The first survey (WMAR),  
177 conducted between 29th January and 19th February 2012, consisted of a grid of 5 by 5  
178 CTD stations with 12 mile (22 km) spacing. The stations at the corners and centres of  
179 the sides as well as the Central Station were to full depth, while the intermediate stations  
180 were to 500 m. There was an extension of 6 stations to the northwest to 1500 m depth.  
181 The Central Station at 51° 12'S, 12° 40'W, was repeated 7 times and a few others twice.  
182 A station at 52°S, 12°W and two in the NW extension region, all completed before the  
183 survey began, have been included in the mapping. The second survey (GeoB), conducted  
184 between 24th February and 3rd March 2012, was centred on 50° 48'S, 38° 12'W, and con-  
185 sisted of 5 meridional sections of 6 CTD stations 24 miles (44 km) apart, both east-west  
186 and north-south, to 1000 m depth.

187  
188 During both cruises hydrographic data were obtained using a Sea-Bird Electronics SBE  
189 911plus Conductivity, Temperature and Depth (CTD) sonde. The sensors were cali-  
190 brated at the factory before and after the cruise, the temperature sensors to a final error  
191 of approximately 0.001 °C and the pressure sensor to 0.01%. The CTD was mounted in  
192 a multi-bottle water sampler type Sea-Bird SBE 32 Carousel holding 24 12-litre bottles,  
193 though in ANTXXVIII/3 two bottles were replaced by an RDI LADCP (Strass et al.  
194 2001, 2017a). Salinities derived from the CTD measurements were later recalibrated by  
195 comparison with salinity samples taken from the water bottles, which were analyzed using  
196 a laboratory salinometer to an uncertainty generally below 0.001 units on the practical  
197 salinity scale, adjusted to IAPSO Standard Seawater (Smetacek, 2005; Wolf-Gladrow,  
198 2013).

199  
200 For some of the eddy surveys physical data from instruments other than the CTD were  
201 available, such as the free-falling MSS turbulence sonde in EIFEX Eddy 2 (Cisewski et  
202 al. 2008) and in the Eddy-Pump WMAR (Strass et al. 2017a). However, the spatial  
203 coverage of the structures was not as good as the CTD stations. During the Eddy-Pump  
204 Cruise some lowered ADCP data were collected, but again not so systematically as to  
205 be useful; in addition there was a clock offset, which was not exactly known (Strass et

206 al. 2017a). Only the CTD data provided a consistent dataset with the best coverage of  
 207 the four structures described here, so it was decided to restrict this paper to these data.  
 208 Hull-mounted ADCP data were collected throughout the cruises, but generally showed  
 209 the same eddy structures as the CTD data, so that for the sake of brevity these have  
 210 been omitted, but are available in Hibbert et al.(2009) for the ANTXXI/3 EIFEX Cruise  
 211 and Strass et al. (2017a) for the ANTXXVIII/3 Eddy Pump Cruise.

212  
 213 For comparison with the *in situ* hydrographic data the merged altimetric data offered  
 214 on the Aviso website (<http://www.aviso.altimetry.fr/en/data.html>, now hosted by ma-  
 215 rine.copernicus.eu) were used. Extracts of the data for the region of interest were provided  
 216 in user-friendly form by colleagues at the National Oceanography Centre in Liverpool.

217

### 218 3 Methods

219 Three parameters have been used to characterise the mesoscale structures. Firstly the  
 220 Winter Water potential temperature minimum,  $\theta_{min}$ , at each station was determined.  
 221 Secondly, the mean potential density,  $\bar{\sigma}_\theta$  was calculated by taking the average for the  
 222 depth range 100 - 480 m, except for EIFEX Eddy 1 where the lower depth had to be lim-  
 223 ited to 390 m as some casts on the westernmost section barely reached 400 m. Thirdly, the  
 224 layer-thickness contribution to the potential vorticity for the depth range was calculated  
 225 in the using:

$$q = -\frac{f}{\bar{\rho}} \frac{\Delta\sigma_\theta}{\Delta z} \quad (1)$$

226 where  $f$  is the Coriolis parameter,  $\bar{\rho}$  is the mean density of the layer,  $\Delta\sigma_\theta$  the density  
 227 difference over the depth range  $\Delta z$ , 100 - 480 (or 390) m. While this is not the whole  
 228 Ertel potential vorticity, it should be the major contribution on the mesoscale (Fischer  
 229 et al. 1989) and adequate for locating the eddy. The reason for standardising on these  
 230 parameters for this depth range was that some of the CTD casts were only made to 500  
 231 m and so may not have reliably quite reached the UCDW  $\theta_{max}$  and it was desired to  
 232 make use of as many stations as possible to enhance statistical significance.

233

234 To characterise the finescale variability two parameters were used. The CTD data from all  
 235 surveys showed a rich and varied pattern of interleaving structures and ways were sought  
 236 in which this might be quantified. The profiles of potential temperature showed consid-  
 237 erable variability both in the shape of the Winter Water potential temperature minimum  
 238 itself, and also in the character of the profile between this temperature minimum,  $\theta_{min}$ , at  
 239 about 150 m depth and the UCDW  $\theta_{max}$  at about 500 m depth. In this depth range there  
 240 was considerable fluctuation about what might be considered to be a "mean profile". To  
 241 characterise this variability the idea of looking at the root mean square variance about  
 242 a smooth curve was tried. Finding a mathematical curve to approximate the  $\theta_{min}$  itself  
 243 proved very challenging and eventually a fourth order polynomial

$$\theta_i = a_0 + a_1 z_i + a_2 z_i^2 + a_3 z_i^3 + a_4 z_i^4 + \epsilon_i \quad (2)$$

244 was fitted to the potential temperature in the depth range between  $\theta_{min}$  and 480 m (or  
 245 390 m for EIFEX Eddy 1) minimising  $\overline{\epsilon_i^2}$  in the usual way, so that the smoothed or model  
 246 potential temperature was

$$\hat{\theta} = a_0 + a_1z + a_2z^2 + a_3z^3 + a_4z^4 \quad (3)$$

247 and then the root mean square fluctuation about this curve was calculated:

$$\theta_{rms} = \sqrt{\frac{1}{n} \sum (\theta_i - \hat{\theta}(z_i))^2} \quad (4)$$

248 As a way of characterising turbulent overturns the vertical diffusivity based on the Thorpe  
 249 scale (Thorpe 1977),  $K_T$ , was calculated using  $\sigma_\theta$  for the depth range 100 - 480 (or 390)  
 250 m. The Thorpe scale itself,  $L_T$ , is the root mean square displacement of water particles  
 251 when a potential density  $\sigma_\theta$  profile is monotonised by sorting:

$$L_T = \sqrt{\frac{1}{n} \sum (z_i^{sorted} - z_i^{unsorted})^2} \quad (5)$$

252 and

$$K_T = 0.2NL_T^2 \quad (6)$$

253 where N is the Brunt-Väisälä frequency.

254

255 Because of the non-linearity of the equation of state, at the low temperatures encoun-  
 256 tered in the ACC, temperature has virtually no effect on density which is determined  
 257 almost entirely by salinity, so that  $\theta_{rms}$  and  $K_T$  should be reasonably independent one of  
 258 another; using two relatively independent measures of fine-scale variability should give  
 259 more confidence in the results.

260

261 Throughout this paper contoured maps and sections are used to display the structures  
 262 of the mesoscale features described. Because of the different ranges of values in the  
 263 different structures observed, it is not possible to use one colour scheme for the same  
 264 parameter in all diagrams and be able to see the structures clearly. Therefore we have  
 265 not used a uniform colouring system; since the principal purpose of the paper is to  
 266 compare structures, rather than absolute values of the parameters, this should not be too  
 267 much of a hindrance.

## 268 4 Results

269 In this section we will consider our four mesoscale structures in order of apparent age  
 270 starting with the youngest, EIFEX Eddy 1, followed by the Eddy-Pump Georgia Basin  
 271 Survey, then EIFEX Eddy 2 and finally the Eddy-Pump West Mid-Atlantic Ridge Survey.

### 272 4.1 EIFEX Eddy 1

273 According to the Aviso Data (<http://www.aviso.altimetry.fr/en/data.html>) this feature  
 274 is only two to three weeks old, and so is still very young (Hibbert et al. 2009)(see Sup-

275plementary Material 1\_EIFEX\_Eddy\_1.mov).

276

277 Maps of mesoscale and finescale quantities are shown in Figure 3. The WW potential  
278 temperature minimum,  $\theta_{min}$ , (a) stretches from the SW corner into the centre of the  
279 survey area with a coldest temperature of about 0.4°C. The mean density,  $\bar{\sigma}_\theta$ , shows  
280 the reverse with a maximum where the water is coldest. The potential vorticity,  $q$ , (b)  
281 shows a minimum in the centre of the survey area, corresponding to the coldest water,  
282 with less negative values surrounding it; in the Southern Hemisphere potential vorticity is  
283 negative and more negative potential vorticity represents a cyclonic feature with negative  
284 vorticity and a cold core. The root-mean-square potential temperature fluctuations,  $\theta_{rms}$   
285 (c) shows maxima where the water is coldest. The Thorpe-scale based diffusivity  $K_T$  (d)  
286 shows larger values in the colder water.  $K_T$  has values in the range  $1 \times 10^{-4}$  to  $1 \times 10^{-3}$   
287  $m^2 s^{-1}$

288

289 Plots of parameters for the ANTXXI/3 EIFEX Eddy 1 Survey as a function of the dis-  
290 tance from the eddy centre at 49.75°S, 18.30°E including the regression line are shown  
291 in Figure 4. The potential temperature at the Winter Water potential temperature  
292 minimum,  $\theta_{min}$  in °C, (a) shows a positive correlation with distance (R=0.360, p=0.005),  
293 while the potential vorticity calculated for the depth range 100-390m in  $rad s^{-1} Gm^{-1}$  (b)  
294 shows no significant correlation with distance from the eddy centre (R=0.037, p=0.778).  
295 Both the root mean square variability of potential temperature  $\theta_{rms}$  in K (c) (R=-0.134,  
296 p=0.328) and the vertical diffusivity based on the Thorpe-scale  $K_T$  in  $m^2 s^{-1}$  (d) (R=-  
297 0.250, p=0.054) show weak decreases with distance from the centre.

298

299 Meridional sections of potential temperature and density along 18°20'E through the eddy  
300 centre are shown in Figure 5. The lens of cold Winter Water can be seen in the latitude  
301 range 49.5 to 50.0 °S and depth range 100 to 300 m. Indeed two separate cores of the  
302 coldest water can be seen, one at 49.6°S and 250 m depth, and the other at 49.75°S and  
303 about 175 m depth. The isopycnals show a distinct doming centred under the cold WW  
304 lens. The non-linearity of the equation of state means that, at the temperatures encoun-  
305 tered, density is determined almost entirely by salinity and temperature is effectively a  
306 passive tracer. Because the isohalines and isopycnals look virtually identical we have not  
307 included salinity sections.

308

309 In the  $\theta S$  diagram, Figure 6, a wide variety of profiles can be seen with potential temper-  
310 ature minima ranging from about 0.5 °C up to about 3.0 °C. The profiles at the centre  
311 of the eddy are shown in dark blue, but the variety of shades, with lighter ones further  
312 from the centre, shows that the eddy core is relatively inhomogeneous.

313

## 314 4.2 Eddy-Pump Georgia Basin Survey (EP GeoB)

315 Looking at at the Aviso Data (<http://www.aviso.altimetry.fr/en/data.html>) sequence in  
316 the period leading up to the Survey it can be seen that cyclonic features are being re-  
317 peatedly formed in the topographically steered flow to the west of the survey area and  
318 being injected into this area from the west. In this particular case the eddy-like feature



319 becomes apparent about the middle of January and our survey was at the end of February  
320 and beginning of March, so that the eddy when investigated was perhaps six weeks old  
321 (see Supplementary Material 2\_Georgia\_Basin.mov).

322

323 The WW  $\theta_{min}$  distribution in the Georgia Basin Survey (Figure 7a) shows that the  
324 area is dominated by a large cold-core structure with warmer water along the northern  
325 and eastern margins, though here there seem to be poorly resolved smaller scale struc-  
326 tures. The occurrence of broad topographically-controlled meanders in this region is  
327 well-documented (Peterson and Whitworth 1989, Orsi et al. 1995); the Aviso sequence  
328 suggests that they continually reform in the same position. The coldest waters have a  
329  $\theta_{min}$  less than 0.4 °C, while the least cold  $\theta_{min}$  in the NE corner is about 2.4 °C. The  
330 mean density  $\bar{\sigma}_\theta$  shows denser water dominating the centre, west and south of the area  
331 with lighter water in the NW and NE corners and on the eastern boundary. The potential  
332 vorticity,  $q$  (b), also shows the same structure with more negative values in the centre,  
333 west and south and less negative values in the NW, NE and on the eastern boundary. The  
334 horizontal distribution of  $q$  indicates that the cold and dense cores are associated with  
335 cyclonic circulation which dominates the area surveyed with smaller meanders around  
336 the northern and eastern rim.

337

338 The variability of potential temperature as measured by  $\theta_{rms}$  (c) shows larger values south  
339 and east of the centre of the eddy. The vertical diffusivity based on the Thorpe-scale,  
340  $K_T$  (d), has values in the range  $1 \times 10^{-4}$  to  $3 \times 10^{-3} m^2 s^{-1}$  with isolated maxima both  
341 in the centre and to the east of the centre of the eddy.

342

343 Figure 8 shows parameters for the ANTXXVIII/3 Eddy-Pump Georgia Basin Survey as a  
344 function of the distance from the eddy centre at 49.80°S, 38.75°W including the regression  
345 line. Potential temperature at the Winter Water potential temperature minimum,  $\theta_{min}$   
346 in °C (a) (R=0.585, p=0.0004) and potential vorticity calculated for the depth range 100-  
347 480m in  $rad s^{-1} Gm^{-1}$  (b) (R=0.510, p=0.003) both show significant correlations with  
348 distance from the eddy centre. The root mean square variability of potential temperature  
349  $\theta_{rms}$  in K (c) (R=-0.337, p=0.060) and the vertical diffusivity based on the Thorpe-scale  
350  $K_T$  in  $m^2 s^{-1}$  (d) (R=-0.362, p=0.042) both show significant negative correlations with  
351 distance from the eddy centre.

352

353 In Figure 9 the section of potential temperature and density along 38°48'W, through the  
354  $\theta_{min}$  minimum and the  $\bar{\sigma}_\theta$  maximum, is shown. The lens of cold WW can be seen centred  
355 between 49.5 and 50.0°S with up-domed isopycnals beneath, but a flattening or M-shaped  
356 structure above.

357

358 The  $\theta S$  diagram in Figure 10 shows a broad range of profiles with WW  $\theta_{min}$  ranging from  
359 about 0.2°C up to about 2.0°C with incipient salinity minima at about 34.1 and 2-3°C  
360 indicating the proximity of the Sub-Antarctic Front at which the Antarctic Intermediate  
361 Water subducts. The profiles at the centre of the eddy are shown in dark blue, and, with  
362 some exceptions, the profiles further away from the centre, shown in lighter shades, are  
363 warmer and saltier.

364

### 4.3 EIFEX Eddy 2

This feature is reckoned to be about six months old by Hibbert et al. (2009) based on the Aviso Data (<http://www.aviso.altimetry.fr/en/data.html>)(see Supplementary Material 3 EIFEX Eddy 2.mov).

All three mesoscale parameters,  $\theta_{min}$ ,  $\bar{\sigma}_\theta$  and  $q$ , Figure 11(a, b), show a closed cold core eddy centred in the north of the survey area. The coldest temperature in the WW core is about 1.0°C, which is rather warmer than in the two previous examples. Hibbert et al. (2009) reported that mixing processes within the eddy increased the temperature by 0.15 K over a period of 40 days, so that a warming of 0.6 K, compared to the EIFEX Eddy 1 core temperature of 0.4 °C could be accomplished in 160 days, or about 5 months. The cold core corresponds to a density maximum and potential vorticity minimum.

The finescale parameters for EIFEX Eddy 2,  $\theta_{rms}$  Figure 11(c), and  $K_T$  (d), show generally small values in the eddy centre and a series of isolated larger values, mostly dotted around the edge.  $K_T$  has values in the range  $1 \times 10^{-4}$  to  $4 \times 10^{-3} m^2 s^{-1}$ .

Plots of parameters for the ANTXXI/3 EIFEX Eddy 2 Survey as a function of the distance from the eddy centre at 49.25°S, 2.25°E including the regression line are shown in Figure 12. Potential temperature at the Winter Water potential temperature minimum,  $\theta_{min}$  in °C (a) (R=0.243, p=0.030) and the potential vorticity calculated for the depth range 100-480m in  $rad s^{-1} Gm^{-1}$  (b) (R=0.246, p=0.028) show significantly positive correlations with distance from the eddy centre. The root mean square variability of potential temperature in pressure coordinates  $\theta_{rms}$  in K (c) (R=0.162, p=0.152) and the vertical diffusivity based on the Thorpe-scale  $K_T$  in  $m^2 s^{-1}$  (d) (R=0.123, p=0.278) show weak positive correlations with distance from the eddy centre.

The section along 2°15'E approximately through the eddy centre, Figure 13, show the thickest part of the WW  $\theta_{min}$  in the latitude range 49.0-49.2°S. Though the isopycnals show a generally broad dome shape, in this range there are signs of a flattening of the isopycnals in the upper water column.

The  $\theta S$  diagram, Figure 14, shows a more ordered relationship than in the previous cases, with a small set of WW  $\theta_{min}$  at about 1°C, more in the range 1.5-2.0°C and then a separate group at about 2.5°C and salinity 34.10-34.15 representing the water immediately outside the eddy. The dark blue curves represent the profiles near the centre of the eddy. The profiles with minima about 1.5°C are paler indicating that they are at some distance away from the eddy centre which is towards the north of the survey area; these profiles come from the col region in the SE where the eddy is still separating from its parental front.

### 4.4 Eddy-Pump West Mid-Atlantic Ridge Survey (EP WMAR)

Looking at the Aviso Data (<http://www.aviso.altimetry.fr/en/data.html>) it can be seen that a anticyclonic feature grows over several weeks in the west of our survey area and

409 reaches a maximum intensity in November 2011 centred at  $51^{\circ}40'S$ ,  $12^{\circ}50'W$ . From then  
410 on it gradually decays and can still be seen on the western boundary of our *in situ* survey  
411 in February 2012 (Figure 15) as a southward meander. To the east of this anticyclone  
412 there are persistent weak cyclonic features, northward meanders, which encroach into  
413 the area as the anticyclone weakens reinvigorating the cyclonic feature in the NW at  
414 the end of December/beginning of January, but the feature we observed *in situ* in Febru-  
415 ary is hard to distinguish at all (see Supplementary Material 4\_Material West\_MAR.mov).

416

417 The hydrographic structure in this survey can be typified by the minimum potential  
418 temperature of the Winter Water,  $\theta_{min}$ , shown in Figure 15a. The main part of the  
419 survey area shows a warmer, southward, poleward meander ("ridge") in the west and a  
420 cooler, northward, equatorward meander ("trough") in the east with the survey covering  
421 virtually one zonal wavelength. Within the trough is a closed  $\theta_{min}$  contour with a value  
422 less than  $1.3^{\circ}C$ . The northwest extension has the least cold water with  $\theta_{min} > 1.9^{\circ}C$ .  
423 The mesoscale parameter  $q$  (Figure 15b) shows a similar structure. The ridge shown by  
424 warmer temperatures has less negative potential vorticity, while the trough shown by  
425 cooler temperatures has more negative potential vorticity with a minimum indicating a  
426 cyclonic centre. The mean density,  $\bar{\sigma}_{\theta}$  shows very weak contrast with high density in  
427 the SE and low values to the NW with the hint of a closed feature near the  $\theta_{min}$  and  
428  $q$  minima; this feature is a density minimum, as can be seen in the section, Figure 17,  
429 discussed below.

430

431 The measures of finescale temperature variability,  $\theta_{rms}$ , (Figure 15c) shows greater vari-  
432 ability on the boundary between the warmer and colder water. The vertical diffusivity  
433 based on the Thorpe scale  $K_T$  (Figure 15h) shows values in the range  $2 \times 10^{-4}$  to  $1 \times 10^{-3}$   
434  $m^2 s^{-1}$  and its spatial structure shows one high value on the boundary between the  
435 warmer and cooler water, though not at the same position as  $\theta_{rms}$ , and higher values in  
436 the east, of which there is only a hint in the other parameters.

437

438 Figure 16 shows parameters for the ANTXXVIII/3 Eddy-Pump West Mid-Atlantic Ridge  
439 Survey as a function of the distance from the eddy centre at  $51.20^{\circ}S$ ,  $12.30^{\circ}W$  including  
440 the regression line. Potential temperature at the Winter Water potential temperature  
441 minimum,  $\theta_{min}$  in  $^{\circ}C$  (a) ( $R=0.346$ ,  $p=0.023$ ) shows a significant positive correlation  
442 with distance from the eddy centre while potential vorticity calculated for the depth  
443 range 100-480m in  $rad s^{-1} Gm^{-1}$  (b) ( $R=0.129$ ,  $p=0.410$ ) shows a weak positive correla-  
444 tion with distance. The root mean square variability of potential temperature in pressure  
445 coordinates  $\theta_{rms}$  in K (c) ( $R=-0.422$ ,  $p=0.005$ ) shows a significant negative correlation  
446 with distance, but with highest values at a range of 25 km, while the vertical diffusivity  
447 based on the Thorpe-scale  $K_T$  in  $m^2 s^{-1}$  (d) ( $R=-0.215$ ,  $p=0.166$ ) shows only a weak  
448 negative correlation.

449

450 The section along  $12^{\circ}20'W$ , Figure 17, through the centre of the  $q$  minimum east of  
451 the centre of the survey area (Figure 15), is unfortunately shorter than would have been  
452 ideal, but does show a rather flattened lens of the WW  $\theta_{min}$ . The isopycnals below this  
453 temperature minimum are bowed downwards, rather than upwards, in this case.

454

455 The  $\theta$ S diagram for this survey, Figure 18, shows a tighter relationship than in all the  
456 other cases with the WW  $\theta_{min}$  in the range 1.1-1.9°C. Profiles from close to the centre in  
457 darker colours and those further away in paler colours are bundled together.

458

## 459 5 Discussion

460 During the Eddy Pump (ANTXXVIII/3) Cruise we observed that the interleavings were  
461 different in magnitude from place to place and wondered whether they were particularly  
462 strong in any part of the eddies. However, we found that they were different from eddy  
463 to eddy. By looking back at the earlier EIFEX (ANTXXI/3) dataset, in which we had  
464 already considered the evolution of some eddy characteristics, and estimating the ages  
465 using altimeter data, we gained the impression that the age of the eddy could be used to  
466 explain the differences observed. This has allowed us to develop a hypothesis about how  
467 eddies evolve.

468

469 The mesoscale parameters,  $\theta_{min}$  and  $q$ , for all four eddy features (Figure 3(a, b), Fig-  
470 ure 7(a, b), Figure 11(a, b), Figure 15(a, b)) show a cyclonic cold WW core  $\theta_{min}$  and  
471 more negative potential vorticity  $q$ . The first three (EIFEX Eddy 1, EP GeoB and EIFEX  
472 Eddy 2) also show a denser core,  $\bar{\sigma}_\theta$ , indicating an upward doming of the isopycnals, as  
473 can be seen in the cross-sections through the eddies (Figure 5, Figure 9 and Figure 13).  
474 However, the last example (EP WMAR) does not share this because, within the depth  
475 range observed, the isopycnals are bowed slightly downwards in the centre of the eddy  
476 beneath the WW  $\theta_{min}$  (Figure 17), though the WW  $\theta_{min}$  and more negative potential  
477 vorticity  $q$  indicate this is, or was, a cyclonic feature. These all show the cold WW  $\theta_{min}$   
478 but with core temperatures of about 0.4°C (EIFEX Eddy 1), 0.4°C (EP GeoB), 1.0°C  
479 (EIFEX Eddy 2) and 1.3°C (EP WMAR). These eddies all formed between the Antarctic  
480 Polar Front and the Southern Polar Front, so that their initial temperatures might be  
481 expected to be similar and the increasing temperature a sign of increasing age as reported  
482 by Hibbert et al. (2009), with a warming rate of about 0.1 K per month.

483

484 Another dataset of interest to the analysis presented here is the survey of the cold core  
485 eddy used in the "EisenEx" iron fertilisation experiment, *Polarstern* Cruise ANTXXVIII/2  
486 from 25th October to 3rd December 2000 (Strass et al. 2001), where CTD data were col-  
487 lected along five meridional sections across the eddy using a towed Scanfish. The depth  
488 range was limited to about 220 m, only just capturing the WW  $\theta_{min}$ , so that the anal-  
489 yses of the lowered CTD data presented for the other eddies could not be carried out.  
490 However, the section through the middle of the eddy at 20°45'E (Figure 19) shows steep  
491 isopycnal slopes at the edge and flattened isopycnals in the centre, more consistent with  
492 that of the older eddies. The core temperature is about 1.2°C, likewise indicating a more  
493 mature structure. The altimeter data show a rather complicated history. A cyclonic  
494 feature becomes established here in June 2000. During July it wanders to the southern  
495 boundary of this area, but returns. At the beginning of October it joins another cyclonic  
496 feature approaching from the west, which eventually replaces it (see Supplementary Ma-  
497 terial 5\_EisenEx\_Eddy.mov).

498

499 The finescale potential temperature parameter  $\theta_{rms}$  (Figure 3(c), Figure 7(c), Figure 11(c)  
500 and Figure 15(c)) shows a variety of different distributions. The first survey (EIFEX Eddy  
501 1) show greater rms variability of potential temperature  $\theta_{rms}$  in the core of the eddy. The  
502 next survey (EP GeoB) shows a maximum off centre and the last two, (EIFEX Eddy 2  
503 and EP WMAR) show greater variability around the edge of the cold core.

504

505 In the recently formed cyclonic eddy with a cold WW core observed by Joyce et al. (1981)  
506 in Drake Passage, they report enhanced interleaving around the edge of the eddy, as do  
507 Adams et al. (2017) from a new eddy in the Scotia Sea, though their data does not  
508 include the eddy centre; our younger eddies show more variability in the centre. In their  
509 study of anticyclonic lenses of Mediterranean Outflow Water ("Meddies") in the North  
510 Atlantic Armi and Zenk (1984) also comment on the enhanced finescale variability round  
511 the edge of the eddy and reduced variability in the centre as do Pietri and Karstensen  
512 (2018) for an SCV in the eastern tropical North Atlantic; by comparison these features  
513 are very old, maybe even years; this result agrees better with our observations.

514

515 The vertical eddy diffusivity based on the Thorpe scale method,  $K_T$ , (Figure 3(d), Fig-  
516 ure 7(d), Figure 11(d) and Figure 15(d)) shows largest values within the eddy core in  
517 the first case (EIFEX Eddy 1). In the second case (EP GeoB) the largest value is in the  
518 core, though there are local maxima around the edge. In the third case (EIFEX Eddy  
519 2) there are local maxima around the edge of the eddy, while in the fourth case (EP  
520 WMAR) the largest values are away from the core of the small weak eddy feature. In all  
521 four surveys the values of  $K_T$  in the upper thermocline are roughly in the range  $10^{-4}$  to  
522  $10^{-3} \text{ m}^2 \text{ s}^{-1}$ . This is in reasonable agreement with measurements made using the MSS  
523 free-falling turbulence sonde during the EIFEX and Eddy-Pump cruises as well as the  
524 earlier EisenEx cruise (Cisewski et al. 2005, Cisewski et al. 2008, Strass et al. 2017). The  
525 values presented here were simply obtained using the processed CTD data, rather than  
526 using the more detailed analysis techniques based on raw data as advocated by Gargett  
527 and Garner (2008), so they may not be such a good estimate of  $K_T$ . However in this  
528 study we are more concerned with the spatial distribution of the fine scale variability  
529 and it is interesting to see that they do agree with the  $\theta_{rms}$  distributions in both the  
530 younger and older eddies. The shift of the  $K_T$  maximum to the rim of the eddies as  
531 they age supports the idea that this is where the stronger shears are concentrated in the  
532 older eddies. Because of the enhanced horizontal density gradient there will be, due to  
533 the geostrophic relationship, enhanced vertical shear, which in its turn provides greater  
534 opportunity for overturnings.

535

536 The diagrams showing the values of parameters as a function of distance from the eddy  
537 centre (Figure 4, Figure 8, Figure 12 and Figure 16) all show  $\theta_{min}$  increasing and  $q$  be-  
538 coming less negative away from the centre (a, b). The first two cases (EIFEX Eddy 1  
539 and EP GeoB) show both  $\theta_{rms}$  and  $K_T$  decreasing away from the eddy centre, while the  
540 third case (EIFEX Eddy 2) shows both of these measures increasing away from the eddy  
541 centre. The fourth case (EP WMAR) shows the largest values of  $\theta_{rms}$  and  $K_T$  in the  
542 distance range 25-50 km which corresponds to the distance to the eddy centre of the  
543 weak frontal feature which runs across the area. The large number of data points there

544 are due to the repeated measurements made at the "central station" of this survey area  
545 at 51°12'S, 12°40'W, the temporal development at which is documented in Strass et al.  
546 (2017).

547

548 The  $\theta S$  diagrams (Figure 6, Figure 10, Figure 14 and Figure 18) show a general trend from  
549 case to case, EIFEX Eddy 1 → EP GeoB → EIFEX Eddy 2 → EP WMAR, of reduced  
550 variability and greater organisation, which would be consistent with a general homogeni-  
551 sation of water mass properties within the core of the eddy as time passes, though it  
552 should be noted that while the first three surveys extended to about 160 km from their  
553 notional centre, the last one only extended to about 120 km. Also the profiles from the  
554 centres of the eddies, as depicted by the dark blue curves, show the "knee" of the Winter  
555 Water becoming less pronounced. As explained by Hibbert et al. (2009) homogenisation  
556 is effected principally by lateral or isopycnic stirring and mixing processes; diapycnic  
557 mixing alone would only warm the local  $\theta_{min}$  values without homogenising them.

558

559 As witnessed by those eddies discussed here, and seen more generally in Chelton et al.'s  
560 (2011) statistics, eddies have a life time of weeks to months. Figure 20 shows the tracks of  
561 four APEX floats on 31st May 2004 originally released in EIFEX Eddy 2 on 14th and 17th  
562 March 2004. The float at 300 m depth crossed the 3°E meridian on 24th April, while the  
563 floats at 200, 500 and 1000 m crossed it on 27th, 25th and 24th May respectively indicat-  
564 ing a collapse of the eddy just over two months following the end of the experiment. This  
565 eddy life time is comparable to the natural time scale of plankton blooms in the ACC,  
566 which is weeks (Smetacek et al. 2012, Soppa et al. 2016, Hoppe et al. 2017). Thus the  
567 homogenisation of physical properties within the eddy described here will be important  
568 for biogeochemical properties and distributions too. Nutrients may become depleted, so  
569 that during the relatively long life time of the eddies the rate at which productivity can  
570 proceed will be constrained by vertical diffusive fluxes.

571

## 572 6 Conclusions

573 Our youngest eddy shows isopycnals which are domed upwards and a variety of waters  
574 with differing temperature-salinity characteristics in its core. The older eddies show cores  
575 which are increasingly homogeneous with age. The isopycnals in the older eddies are more  
576 flattened in the centre of the eddy and in cross-section they can be M-shaped, so that the  
577 steepest gradients are concentrated around the rim of the eddy. We hypothesise that stir-  
578 ring and mixing processes within the eddy are likely to homogenise the water so that the  
579 temperature-salinity relationship becomes tighter. Fine scale variability, characterised  
580 by  $\theta_{rms}$  and  $K_T$ , which is spread throughout the youngest eddy, becomes concentrated  
581 around the edges of the older eddies, so that younger eddies have more variability in the  
582 centre and older eddies more round the edge.

583

584 To test our hypothesis about how eddies evolve properly would require detailed study of  
585 a series of similar eddies with different ages. As is so often in ocean science the dataset  
586 available to us was not ideal and new experiments collecting more systematic datasets

587 would probably be needed. This might not be so simple. Argo floats are probably too  
588 sparse, but have essentially vertical profiles. Gliders and towed systems would be inclined  
589 to muddle horizontal and vertical variability, so that a number of time-consuming high-  
590 resolution CTD surveys might be required. Alternatively, by combining Argo float data  
591 with altimeter data it might be possible to test our hypothesis, if sufficient profiles could  
592 be found and their positions relative to the centre of eddies of known age determined.

593  
594 The sharpened front-like gradients around the edge offer the opportunity for baroclinic  
595 and barotropic instability to cause the eddy to collapse and release the water it has  
596 homogenised back into the general flow, as illustrated by the release of the floats from  
597 EIFEX Eddy 2 (Figure 20). We can see from this how the formation of eddies, homogeni-  
598 sation of properties within them and the release of this modified water could contribute  
599 to the way in which ocean processes are changing water mass characteristics.

600  
601 The correct representation of the processes described in this paper is going to be im-  
602 portant for modelling not only of the bulk rate at which the ocean is converting and  
603 exchanging water mass properties such as heat and fresh water but also of biogeochemi-  
604 cal processes which depend on this physical context.

605

## 606 **7 Acknowledgements**

607 We should like to thank the German Federal Ministry for Education and Research (Bun-  
608 desministerium für Bildung und Forschung, BMBF) for funding *Polarstern* and this ship's  
609 captains and crews. HL's travel costs were born by the Royal Society (ANTXVIII/2, AN-  
610 TXXI/3) and the School of Environmental Sciences (ANTXXVIII/3). Our thanks are  
611 due to Chris Hughes and Angela Hibbert at the National Oceanography Centre in Liv-  
612 erpool for extracts of the Aviso merged altimetric data set and to Santiago Gonzalez at  
613 NIOZ for the data from the Scanfish towed system (ANTXVIII/2).

614

## 615 **8 References**

616 Adams, K. A., P. Hosegood, J. R. Taylor, J.-B. Sallée, S. Bachman, R. Torres and M.  
617 Stamper, 2017, Frontal circulation and submesoscale variability during the formation of a  
618 Southern Ocean mesoscale eddy. *J. Phys. Oceanogr.*, 47, 1737-1753. DOI: 10.1175/JPO-  
619 D-16-0266.1.

620

621 Armi, L., and W. Zenk, 1984, Large lenses of highly saline Mediterranean Water. *J.*  
622 *Phys. Oceanogr.*, 14, 1560-1576.

623

624 Behrenfeld, M. J., 2010, Abandoning Sverdrup's critical depth hypothesis on phytoplank-  
625 ton blooms. *Ecology*, 91, 977-989.

626

627 Bopp, L., M. Lévy, L. Resplandy, and J. B. Sallée (2015), Pathways of anthropogenic car-  
628 bon subduction in the global ocean, *Geophys. Res. Lett.*, 42, 6416–6423, doi:10.1002/2015GL065073.  
629

630 Charney, J. G., 1947, The dynamics of long waves in a baroclinic westerly current. *J.*  
631 *Meteor.*, 4, 135-162.  
632

633 Chelton, D. B., M. G. Schlax, and R. M. Samelson, 2011, Global observations of nonlin-  
634 ear mesoscale eddies. *Progress in Oceanography*, 91(2), 167-216.  
635 <http://dx.doi.org/10.1016/j.pocean.2011.01.002>.  
636

637 Cisewski, B., V. H. Strass and H. Prandke, 2005, Upper-ocean vertical mixing in the  
638 Antarctic Polar Front Zone. *Deep-Sea Res. II*, 52, 1087-1108. doi: 10.1016/j.dsr2.2005.01.010.  
639

640 Cisewski, B., V. H. Strass, M. Losch and H. Prandke, 2008, Mixed layer analysis of  
641 a mesoscale eddy in the Antarctic Polar Front Zone. *J. Geophys. Res.*, 113, C05017,  
642 doi:10.1029/2007JC004372.  
643

644 D'Asaro, E. A., 1988, Generation of Submesoscale Vortices: A New Mechanism. *J. Geo-*  
645 *phys. Res.*, 93, 6685-6693.  
646

647 Eady, E. T., 1949, Long waves and cyclone waves. *Tellus*, 1, 258-277.  
648

649 Edmon, H. J., B. J. Hoskins and M. E. McIntyre, 1980, Eliassen-Palm cross-sections for  
650 the troposphere. *J. Atmos. Sci.*, 37, 2600-2616 (see also Corrigendum, *J. Atmos. Sci.*,  
651 38, 1115, 1980).  
652

653 Fischer, J., H. Leach and J.D. Woods, 1989, A synoptic map of isopycnic potential vor-  
654 ticity in the seasonal thermocline. *J. Phys. Oceanogr.*, 19, 519-531.  
655

656 Gargett, A., and T. Garner, 2008, Determining Thorpe Scales from Ship-Lowered CTD  
657 Density Profiles. *J. Atmos. and Ocean. Tech.*, 25, 1657-1670. DOI: 10.1175/2008JTE-  
658 CHO541.1.  
659

660 Gill, A. E., J. S. A. Green and A. J. Simmons, 1974, Energy partition in the large-scale  
661 ocean circulation and the production of mid-ocean eddies. *Deep-Sea Res.*, 21, 499-528.  
662

663 Gordon, A. L., 1971, Antarctic Polar Front Zone. *Antarctic Oceanology*, Vol. 1, Antarc-  
664 tic Research Series, J. L. Reid, Ed., Amer. Geophys. Union, 205-221.  
665

666 Gordon, A. L., Georgi, D. T., and Taylor, H. W., 1977, Antarctic Polar Frontal Zone in  
667 the western Scotia Sea - Summer 1975. *Journal of Physical Oceanography*, 7, 309–328.  
668

669 Hibbert, A., H. Leach, V. Strass and B. Cisewski, 2009, Mixing in Cyclonic Eddies  
670 in the Antarctic Circumpolar Current. *Journal of Marine Research*, 67, 1-23. DOI:  
671 10.1357/002224009788597935.  
672



673 Hoppe, C. , Klaas, C. , Ossebaar, S. , Soppa, M. A. , Cheah, W. , Laglera, L. , Santos-  
674 Echeandia, J. , Rost, B. , Wolf-Gladrow, D. , Bracher, A. , Hoppema, M. , Strass, V.  
675 and Trimborn, S., 2017, Controls of primary production in two phytoplankton blooms  
676 in the Antarctic Circumpolar Current, Deep Sea Research Part II: Topical Studies in  
677 Oceanography, 138 , 63-73. doi:10.1016/j.dsr2.2015.10.005

678

679 Ito T., P. Parekh, S. Dutkiewicz, and M. J. Follows, 2005, The Antarctic Circumpolar  
680 Productivity Belt. *Geophys. Res. Lett.*, 32, L13604, doi:10.1029/2005GL023021.

681

682 Jones, E.M., Hoppema, M., Strass, V., Hauck, J., Salt, L., Klaas, C., van Heuven  
683 S.M.A.C., Wolf-Gladrow D., de Baar H.J.W., 2017. Mesoscale features create hotspots  
684 of carbon uptake in the Antarctic Circumpolar Current, Deep. Sea Res. Part II: Top.  
685 Stud. Oceanogr. 138, 39–51.

686

687 Joyce, T., 1977, A Note on the Lateral Mixing of Water Masses. *J. Phys. Oceanogr.*, 7,  
688 626-629.

689

690 Joyce, T., W. Zenk and J. M. Toole, 1978, The anatomy of the Antarctic Polar Front in  
691 the Drake Passage. *J. Geophys. Res.*, 83, 6093-6113.

692

693 Joyce, T. M., S. L. Patterson, and R. C. Millard, 1981, Anatomy of a cyclonic ring in the  
694 Drake Passage, *Deep Sea Res.*, 28, 1265-1287.

695

696 Kurczyn, J. A., E. Beier, M. F. Lavín, A. Chaigneau and V. M. Godínez, 2013, Anatomy  
697 and evolution of a cyclonic mesoscale eddy observed in the northeastern Pacific tropical-  
698 subtropical transition zone, *J. Geophys. Res. Oceans*, 118, 5931–5950, doi:10.1002/2013JC009339.

699

700 Leach, H., V. H. Strass and B. Cisewski, 2011, Modification by Lateral Mixing of the  
701 Warm Deep Water entering the Weddell Sea in the Maud Rise Region. *Ocean Dynamics*,  
702 61, (1), 51-68. DOI: 10.1007/s10236-010-0342-y

703

704 MacVean, M. K., and J. D. Woods, 1980, Redistribution of scalars during upper ocean  
705 frontogenesis. *A numerical Model. Quart. J. Roy. Met. Soc.* 106, 293-311.

706

707 Marshall, J., and K. Speer, 2012, Closure of the meridional overturning circulation  
708 through Southern Ocean upwelling. *Nature Geoscience*, 5, 171-180. doi: 10.1038/NNGEO1391.

709

710 Martin, J. H., 1990, Glacial-interglacial CO<sub>2</sub> change: the iron hypothesis. *Paleoceanog-*  
711 *raphy*, 5, 1-13.

712

713 McWilliams, J. C., 1985, Submesoscale, coherent vortices in the ocean. *Rev. Geophys.*,  
714 23, 165-182.

715

716 Methven, J., 1998, Spirals in Potential Vorticity. Part II: Stability. *J. Atmos. Sci.*, 55,  
717 2067-2079.

718

719 Methven, J., and B. J. Hoskins, 1998, Spirals in Potential Vorticity. Part 1: Measures of  
720 Structure. *J. Atmos. Sci.*, 55, 2053-2066.

721

722 Methven, J., and B. J. Hoskins, 1999, The advection of high-resolution tracers by low-  
723 resolution winds. *J. Atmos. Sci.*, 56, 3262-3285.

724

725 Meunier, T., C. Ménesguen, R. Schopp and S. le Gentil, 2015, Tracer stirring around a  
726 Meddy: The formation of layering. *J. Phys. Oceanogr.*, 45, 407-423. DOI: 10.1175/JPO-  
727 D-14-0061.1

728

729 MODE-Group, 1978: The Mid-Ocean Dynamics Experiment. *Deep-Sea Res.*, 25, 859-910.

730

731 Molemaker, M. J., J. C. McWilliams and W. K. Dewar, 2015, Submesoscale instability  
732 and generation of mesoscale anticyclones near a separation of the California Undercur-  
733 rent. *J. Phys. Oceanogr.*, 45, 613-629. DOI: 10.1175/JPO-D-13-0225.1.

734

735 Moore, J. K., and M. R. Abbott, 2000, Phytoplankton chlorophyll distributions and pri-  
736 mary production in the Southern Ocean. *J. Geophys. Res.*, 105, 28,709-28,722.

737

738 Moore, J. K., and M. R. Abbott, 2002, Surface chlorophyll concentrations in relation to  
739 the Antarctic Polar Front: seasonal and spatial patterns from satellite observations. *J.*  
740 *Mar. Systems*, 37, 69-86.

741

742 Munk, W. H., 1950, On the wind-driven circulation. *J. Meteorol.*, 7, 79-93.

743

744 Orsi, A. H., T. Whitworth III, W. D. Nowlin Jr, 1995, On the meridional extent and  
745 fronts of the Antarctic Circumpolar Current. *Deep-Sea Res. I*, 42, 641-673.

746

747 Peterson, R. G., W. D. Nowlin, and T. Whitworth, 1982, Generation and evolution of a  
748 cyclonic ring at Drake Passage in early 1979, *J. Phys. Ocean.*, 12, 712-719.

749

750 Peterson, R.G., and T. Whitworth, 1989, The Subantarctic and Polar Fronts in Relation  
751 to Deep Water Masses through the Southwestern Atlantic . *J. Geophys. Res.*, 94, 10817-  
752 10838.

753

754 Pietri, A., and J. Karstensen, 2018, Dynamical characterisation of a low oxygen subme-  
755 soscale coherent vortex in the eastern North Atlantic Ocean. *J. Geophys. Res.: Oceans*,  
756 123, 2049-2065. DOI: 10.1002/2017JC013177.

757

758 Sallée, J. B., R. J. Matear, S. R. Rintoul, and A. Lenton, 2012, Localized subduction  
759 of anthropogenic carbon dioxide in the Southern Hemisphere oceans, *Nat. Geosci.*, 5(8),  
760 579-584, doi:10.1038/ngeo1523.

761

762 Smetacek, V. 2005. Fahrtabschnitt ANT XXI/3 Kapstadt-Kapstadt. *Ber. Polarforsch.*  
763 *Meeresforsch.*, 500, 1-134.

764

765 Smetacek, V., C. Klaas, V. H. Strass, P. Assmy, M. Montresor, B. Cisewski, N. Savoye,  
766 A. Webb, F. d'Ovidio, J. M. Arrieta, U. Bathmann, R. Bellerby, G. M. Berg, P. Croot,  
767 S. Gonzalez, J. Henjes, G. J. Herndl, L. J. Hoffmann, H. Leach, M. Losch, M. M. Mills,  
768 C. Neill, I. Peeken, R. Röttgers, O. Sachs, E. Sauter, M. M. Schmidt, J. Schwarz, A.  
769 Terbrüggen, and D. Wolf-Gladrow, 2012, Deep carbon export from a Southern Ocean  
770 iron-fertilized diatom bloom. *Nature*, 487, 313-319. doi: 10.1038/nature11229.

771  
772 Smith, K. S., and R. Ferrari, 2009, The production and dissipation of compensated  
773 thermohaline variance by mesoscale stirring. *J. Phys. Oceanogr.*, 39, 2477-2501. doi:  
774 10.1175/2009JPO4103.1

775  
776 Sokolov, S., and S. R. Rintoul, 2009, Circumpolar structure and distribution of the  
777 Antarctic Circumpolar Current fronts: 1. Mean circumpolar paths. *J. Geophys. Res.*,  
778 114, C11018, doi:10.1029/2008JC005108.

779  
780 Soppa, M. , C. Völker, and A. Bracher, 2016, Diatom Phenology in the Southern Ocean:  
781 Mean Patterns, Trends and the Role of Climate Oscillations. *Remote Sensing*, 8 (420),  
782 pp. 1-17. doi:10.3390/rs8050420 , hdl:10013/epic.47911

783  
784 Stommel, H., 1948, The westward intensification of wind-driven ocean currents. *Eos*  
785 *Trans. AGU*, 29, 2002-206. DOI: 10.1029/TR029i002p00202

786  
787 Strass, V. H., H. Leach, B. Cisewski, S. Gonzalez, J. Post, V. da Silva Duarte and F.  
788 Trumm, 2001, The physical setting of the Southern Ocean Iron Fertilisation Experiment.  
789 Chapter 10 in Smetacek, V., U. Bathmann and S. El Naggar, (Eds.), 2001, *The Expedi-*  
790 *tions ANTARKTIS XVIII/1-2 of the Research Vessel "Polarstern" in 2000. Berichte zur*  
791 *Polar- und Meeresforschung*, Nr 400. 232pp.

792  
793 Strass, V.H., A.C. Naveira Garabato, R.T. Pollard, H. I. Fischer, I. Hense, J.T. Allen,  
794 J.F. Read, H. Leach and V. Smetacek, 2002, Mesoscale frontal dynamics: Shaping the  
795 environment of primary production in the Antarctic Circumpolar Current. *Deep-Sea Res.*  
796 *II*, 49 (18), 3735-3770. DOI:10.1016/S0967-0645(02)00109-1

797  
798 Strass, V., B. Cisewski, S. Gonzales, H. Leach, K.-D. Loquay, H. Prandke, H. Rohr, and  
799 M. Thomas, 2005, The physical setting of the European Iron Fertilization Experiment  
800 'EIFEX' in the Southern Ocean, *Rep. Polar Mar. Res.*, 500, 15–49.

801  
802 Strass, V. H., H. Leach, H. Prandke, M. Donnelly, A. U. Bracher and D. A. Wolf-Gladrow,  
803 2017a, The physical environmental conditions for biogeochemical differences along the  
804 Antarctic Circumpolar Current in the Atlantic Sector during late austral summer 2012.  
805 *Deep-Sea Res. II*, 138, 6-25. doi: 10.1016/j.dsr2.2016.05.018

806  
807 Strass, V., E. Pakhomov and D. Wolf-Gladrow [Eds.] 2017b, Eddy-Pump: Pelagic pro-  
808 cesses along the eddying Antarctic Polar Front with influence on the carbon pump in the  
809 Atlantic Sector of the Southern Ocean. *Deep-Sea Res. II*, 138, 1-140.

810

811 Sverdrup, H. U., 1947, Wind-Driven Currents in a Baroclinic Ocean; with Application to  
812 the Equatorial Currents of the Eastern Pacific". Proc. Natl. Acad. Sci. U.S.A. 33 (11):  
813 318–26. doi:10.1073/pnas.33.11.318.

814

815 Swart, N. C., I. J. Ansoorge, and J. R. E. Lutjeharms, 2008, Detailed characterization of  
816 a cold Antarctic eddy, J. Geophys. Res., 113, C01009, doi:10.1029/2007JC004190.

817

818 Thompson, A. F., S. T. Gille, J. A. MacKinnon and J. Sprintall, 2007, Spatial and tem-  
819 poral patterns of small-scale mixing in Drake Passage.

820

821 Thomsen, S., T. Kanzow, G. Krahnemann, R. J. Greatbatch, M. Dengler and G. Lavik,  
822 2016, The formation of a subsurface anticyclonic eddy in the Peru-Chile Undercurrent  
823 and its impact on the near-coastal salinity, oxygen and nutrient distributions. J. Geo-  
824 phys. Res.: Oceans, 121, 476-501. DOI: 10.1002/2015JC010878.

825

826 Wolf-Gladrow, D., [Ed.], 2013, The Expedition of the Research Vessel "Polarstern"  
827 to the Antarctic in 2012 (ANT-XXVIII/3). Ber. Pol. u. Meeresf., 661, 195 pp.  
828 <http://hdl.handle.net/10013/epic.41332>.

829

830 Woods, J. D., R. Onken and J. Fischer, 1986, Thermohaline intrusions created isopyc-  
831 nally at oceanic fronts are inclined to isopycnals. Nature, 322, 446-449.

832

833 Zhang, Z. et al., J. Tian, B. Qiu, W. Zhao, P. Chang, D. Wu and X. Wan, 2016, Ob-  
834 served 3D Structure, Generation, and Dissipation of Oceanic Mesoscale Eddies in the  
835 South China Sea. Sci. Rep. 6, 24349; doi: 10.1038/srep24349

836

## 837 9 Figure Captions

838 Figure 1. Track of *Polarstern* Cruise ANTXXI/3 – "EIFEX" – leaving from Cape Town  
839 on 21st January 2004 and arriving back in Cape Town on 25th March 2004.

840

841 Figure 2. Track of *Polarstern* Cruise ANTXXVIII/3 – "Eddy-Pump" – leaving from  
842 Cape Town on 7th January 2012 and arriving in Punta Arenas on 11th March 2012.

843

844 Figure 3. Maps of parameters for the ANTXXI/3 EIFEX Eddy 1 Survey overlain with  
845 mean potential density  $\overline{\sigma_\theta}$  for the upper thermocline depth range 100-390m with a con-  
846 tour interval of  $0.05 \text{ kg m}^{-3}$  showing a maximum in the middle of the area: (a) potential  
847 temperature at the Winter Water potential temperature minimum,  $\theta_{min}$  in  $^\circ\text{C}$ , (b) po-  
848 tential vorticity calculated for the depth range 100-390m in  $\text{rad s}^{-1} \text{ Gm}^{-1}$ , (c) the root  
849 mean square variability of potential temperature in pressure coordinates  $\theta_{rms}$  in K, (d)  
850 the vertical diffusivity based on the Thorpe-scale  $K_T$  in  $\text{m}^2 \text{ s}^{-1}$ .

851

852 Figure 4. Plots of parameters for the ANTXXI/3 EIFEX Eddy 1 Survey as a function  
853 of the distance from the eddy centre at  $49.75^\circ\text{S}$ ,  $18.30^\circ\text{E}$  including the regression line:

854 (a) potential temperature at the Winter Water potential temperature minimum,  $\theta_{min}$  in  
855  $^{\circ}\text{C}$  ( $R=0.360$ ,  $p=0.005$ ), (b) potential vorticity calculated for the depth range 100-390m  
856 in  $\text{rad s}^{-1} \text{ Gm}^{-1}$  ( $R=0.037$ ,  $p=0.778$ ), (c) the root mean square variability of potential  
857 temperature in pressure coordinates  $\theta_{rms}$  in  $\text{K}$  ( $R=-0.134$ ,  $p=0.328$ ), (d) the vertical dif-  
858 fusivity based on the Thorpe-scale  $K_T$  in  $\text{m}^2 \text{ s}^{-1}$  ( $R=-0.250$ ,  $p=0.054$ ).

859

860 Figure 5. Meridional section through ANTXXI/3 EIFEX Eddy 1 along  $18^{\circ}20'\text{E}$  showing  
861 potential temperature  $\theta$  and overlain with density  $\sigma_{\theta}$  in the top 500 m in white. Note the  
862 lens of cold Winter Water and the corresponding domed isopycnals centred at  $49.75^{\circ}\text{S}$ .  
863 For scale  $1^{\circ}$  of latitude corresponds to 111 km. The station positions are marked by thin  
864 black lines.

865

866 Figure 6. Potential temperature-salinity,  $\theta\text{S}$ , diagram for the ANTXXI/3 EIFEX Eddy  
867 1 Survey. Contours of potential density,  $\sigma_{\theta}$ , are shown in black. Notice the broad range  
868 of local water masses present, in particular the wide variety of Winter Water  $\theta$  minima  
869 from ca.  $0.5^{\circ}\text{C}$  to above  $2.0^{\circ}\text{C}$ . The profiles are coloured by the distance from the eddy  
870 centre at  $49.75^{\circ}\text{S}$ ,  $18.30^{\circ}\text{E}$ .

871

872 Figure 7. Maps of parameters for the ANTXXVIII/3 Eddy-Pump Georgia Basin Survey  
873 overlain with the mean potential density  $\overline{\sigma_{\theta}}$  for the upper thermocline depth range 100-  
874 480m with a contour interval of  $0.05 \text{ kg m}^{-3}$ ; the closed contour is a density maximum:  
875 (a) potential temperature at the Winter Water potential temperature minimum,  $\theta_{min}$  in  
876  $^{\circ}\text{C}$ , (b) potential vorticity calculated for the depth range 100-480m in  $\text{rad s}^{-1} \text{ Gm}^{-1}$ , (c)  
877 the root mean square variability of potential temperature in pressure coordinates  $\theta_{rms}$  in  
878  $\text{K}$ , (d) the vertical diffusivity based on the Thorpe-scale  $K_T$  in  $\text{m}^2 \text{ s}^{-1}$ .

879

880 Figure 8. Plots of parameters for the ANTXXVIII/3 Eddy-Pump Georgia Basin Sur-  
881 vey as a function of the distance from the eddy centre at  $49.80^{\circ}\text{S}$ ,  $38.75^{\circ}\text{W}$  including  
882 the regression line: (a) potential temperature at the Winter Water potential temperature  
883 minimum,  $\theta_{min}$  in  $^{\circ}\text{C}$  ( $R=0.585$ ,  $p=0.000$ ), (b) potential vorticity calculated for the depth  
884 range 100-480m in  $\text{rad s}^{-1} \text{ Gm}^{-1}$  ( $R=0.510$ ,  $p=0.003$ ), (c) the root mean square variabil-  
885 ity of potential temperature in pressure coordinates  $\theta_{rms}$  in  $\text{K}$  ( $R=-0.337$ ,  $p=0.060$ ), (d)  
886 the vertical diffusivity based on the Thorpe-scale  $K_T$  in  $\text{m}^2 \text{ s}^{-1}$  ( $R=-0.362$ ,  $p=0.042$ ).

887

888 Figure 9. Meridional section through the ANTXXVIII/3 Eddy-Pump Georgia Basin  
889 Eddy along  $38^{\circ}48'\text{W}$ , through the  $\theta_{min}$  minimum and the  $\overline{\sigma_{\theta}}$  maximum, showing poten-  
890 tial temperature  $\theta$  and overlain with density  $\sigma_{\theta}$  in the top 500 m in white. Note the lens  
891 of cold Winter Water and the corresponding domed isopycnals centred between  $49.5$  and  
892  $50.0^{\circ}\text{S}$ . For scale  $1^{\circ}$  of latitude corresponds to 111 km. The station positions are marked  
893 by thin black lines.

894

895 Figure 10. Potential temperature-salinity,  $\theta\text{S}$ , diagram for the ANTXXVIII/3 Eddy-  
896 Pump Georgia Basin Eddy Survey. Contours of potential density,  $\sigma_{\theta}$ , are shown in black.  
897 Notice the broad range of local water masses present, in particular the wide variety of  
898 Winter Water  $\theta$  minima from ca.  $0.2^{\circ}\text{C}$  to above  $2.0^{\circ}\text{C}$ . Notice also the incipient salinity  
899 minima in the range 34.0 to 34.1. The profiles are coloured by the distance from the eddy

900 centre at 49.80°S, 38.75°W.

901

902 Figure 11. Maps of parameters for the ANTXXI/3 EIFEX Eddy 2 Survey overlain with  
903 the mean potential density  $\bar{\sigma}_\theta$  for the upper thermocline depth range 100-480m with a  
904 contour interval of 0.05 kg m<sup>-3</sup>; the closed contour is a density maximum: (a) potential  
905 temperature at the Winter Water potential temperature minimum,  $\theta_{min}$  in °C, (b) po-  
906 tential vorticity calculated for the depth range 100-480m in rad s<sup>-1</sup> Gm<sup>-1</sup>, (c) the root  
907 mean square variability of potential temperature in pressure coordinates  $\theta_{rms}$  in K, (d)  
908 the vertical diffusivity based on the Thorpe-scale  $K_T$  in m<sup>2</sup> s<sup>-1</sup>.

909

910 Figure 12. Plots of parameters for the ANTXXI/3 EIFEX Eddy 2 Survey as a function  
911 of the distance from the eddy centre at 49.25°S, 2.25°E including the regression line:  
912 (a) potential temperature at the Winter Water potential temperature minimum,  $\theta_{min}$  in  
913 °C (R=0.243, p=0.030), (b) potential vorticity calculated for the depth range 100-480m  
914 in rad s<sup>-1</sup> Gm<sup>-1</sup> (R=0.246, p=0.028), (c) the root mean square variability of potential  
915 temperature in pressure coordinates  $\theta_{rms}$  in K (R=0.162, p=0.152), (d) the vertical dif-  
916 fusivity based on the Thorpe-scale  $K_T$  in m<sup>2</sup> s<sup>-1</sup> (R=0.123, p=0.278).

917

918 Figure 13. Meridional section through ANTXXI/3 EIFEX Eddy 2 along 2°15'E showing  
919 potential temperature  $\theta$  and overlain with density  $\sigma_\theta$  in the top 500 m in white. Note the  
920 lens of cold Winter Water thickest at about 49.2°S and how the isopycnals there are less  
921 sharply domed. For scale 1° of latitude corresponds to 111 km. The station positions are  
922 marked by thin black lines.

923

924 Figure 14. Potential temperature-salinity,  $\theta S$ , diagram for the ANTXXI/3 EIFEX Eddy  
925 2 Survey. Contours of potential density,  $\sigma_\theta$ , are shown in black. Notice the bundling of  
926 local water masses, in particular the Winter Water  $\theta$  minima below 2.0°C of the water  
927 within the eddy and the distinct group with  $\theta$  minima above 2.0°C outside the eddy core.  
928 The profiles are coloured by the distance from the eddy centre at 49.25°S, 2.25°E.

929

930 Figure 15. Maps of parameters for the ANTXXVIII/3 Eddy-Pump West Mid-Atlantic  
931 Ridge Survey overlain with the mean potential density  $\bar{\sigma}_\theta$  for the upper thermocline depth  
932 range 100-480m with a contour interval of 0.05 kg m<sup>-3</sup>; the closed contour is a density  
933 minimum: (a) potential temperature at the Winter Water potential temperature mini-  
934 mum,  $\theta_{min}$  in °C, (b) potential vorticity  $q$  calculated for the depth range 100-480m in  
935 rad s<sup>-1</sup> Gm<sup>-1</sup>, (c) the root mean square variability of potential temperature in pressure  
936 coordinates  $\theta_{rms}$  in K, (d) the vertical diffusivity based on the Thorpe-scale  $K_T$  in m<sup>2</sup> s<sup>-1</sup>.

937

938 Figure 16. Plots of parameters for the ANTXXVIII/3 Eddy-Pump West Mid-Atlantic  
939 Ridge Survey as a function of the distance from the eddy centre at 51.20°S, 12.30°W  
940 including the regression line: (a) potential temperature at the Winter Water potential  
941 temperature minimum,  $\theta_{min}$  in °C (R=0.346, p=0.023), (b) potential vorticity calculated  
942 for the depth range 100-480m in rad s<sup>-1</sup> Gm<sup>-1</sup> (R=0.129, p=0.410), (c) the root mean  
943 square variability of potential temperature in pressure coordinates  $\theta_{rms}$  in K (R=-0.422,  
944 p=0.005), (d) the vertical diffusivity based on the Thorpe-scale  $K_T$  in m<sup>2</sup> s<sup>-1</sup> (R=-0.215,  
945 p=0.166).

946

947 Figure 17. Meridional section through the ANTX XVIII/3 Eddy-Pump West Mid-Atlantic  
948 Ridge Eddy along  $12^{\circ}20'W$  showing potential temperature  $\theta$  overlain with density  $\sigma_{\theta}$  in  
949 the top 500 m in white. Note the lens of cold Winter Water thickest at  $51.0^{\circ}S$  and how  
950 the isopycnals in this case are actually depressed. For scale  $1^{\circ}$  of latitude corresponds to  
951 111 km. The station positions are marked by thin black lines.

952

953 Figure 18. Potential temperature-salinity,  $\theta S$ , diagram for the ANTX XVIII/3 Eddy-  
954 Pump West Mid-Atlantic Ridge Eddy Survey. Contours of potential density,  $\sigma_{\theta}$ , are  
955 shown in black. Notice the bundling of local water masses, in particular the Winter Wa-  
956 ter  $\theta$  minima in the range  $1.0$  to  $2.0^{\circ}C$ . The profiles are coloured by the distance from  
957 the eddy centre at  $51.20^{\circ}S$ ,  $12.30^{\circ}W$ .

958

959 Figure 19. Meridional sections through the ANTX VIII/2 "EisenEx" cold core eddy along  
960  $20^{\circ}45'E$  showing potential temperature  $\theta$  overlain with density  $\sigma_{\theta}$  in the top 220 m in  
961 white. Note the flattened lens of cold Winter Water centred at at about  $48.0^{\circ}S$  and how  
962 the the isopycnals in this case slope steeply down in the north and south; to the south  
963 they slope up again where the eddy is detaching from its parental front.

964

965 Figure 20. Tracks of four APEX floats on 31st May 2004 originally released in EIFEX  
966 Eddy 2 on 14th and 17th March 2004. The float at 300 m depth crossed the  $3^{\circ}E$  meridian  
967 on 24th April, while the floats at 200, 500 and 1000 m crossed it on 27th, 25th and 24th  
968 May respectively.

969

970

aged03/rev.0033/28.11.2018/HL

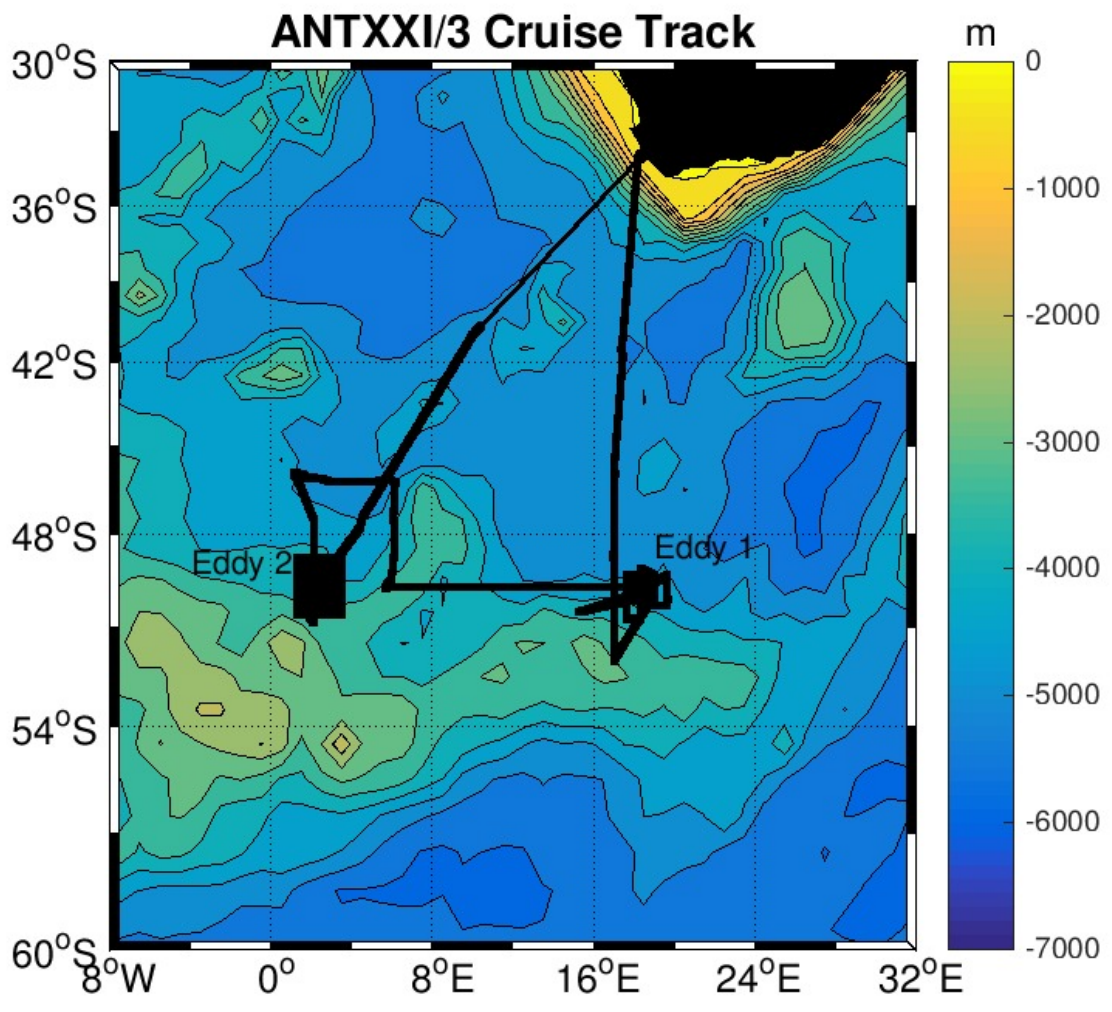


Figure 1



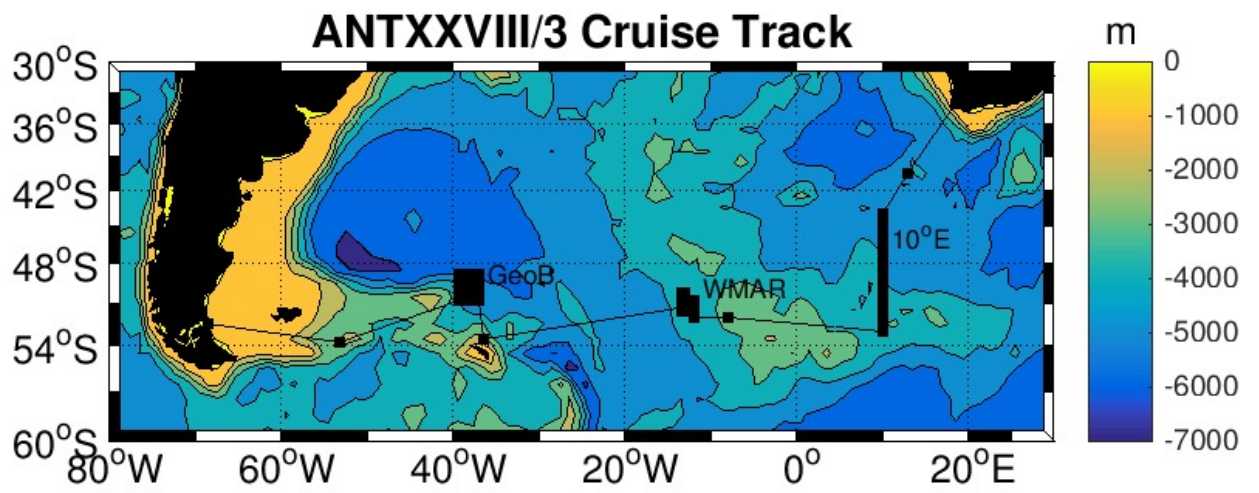


Figure 2

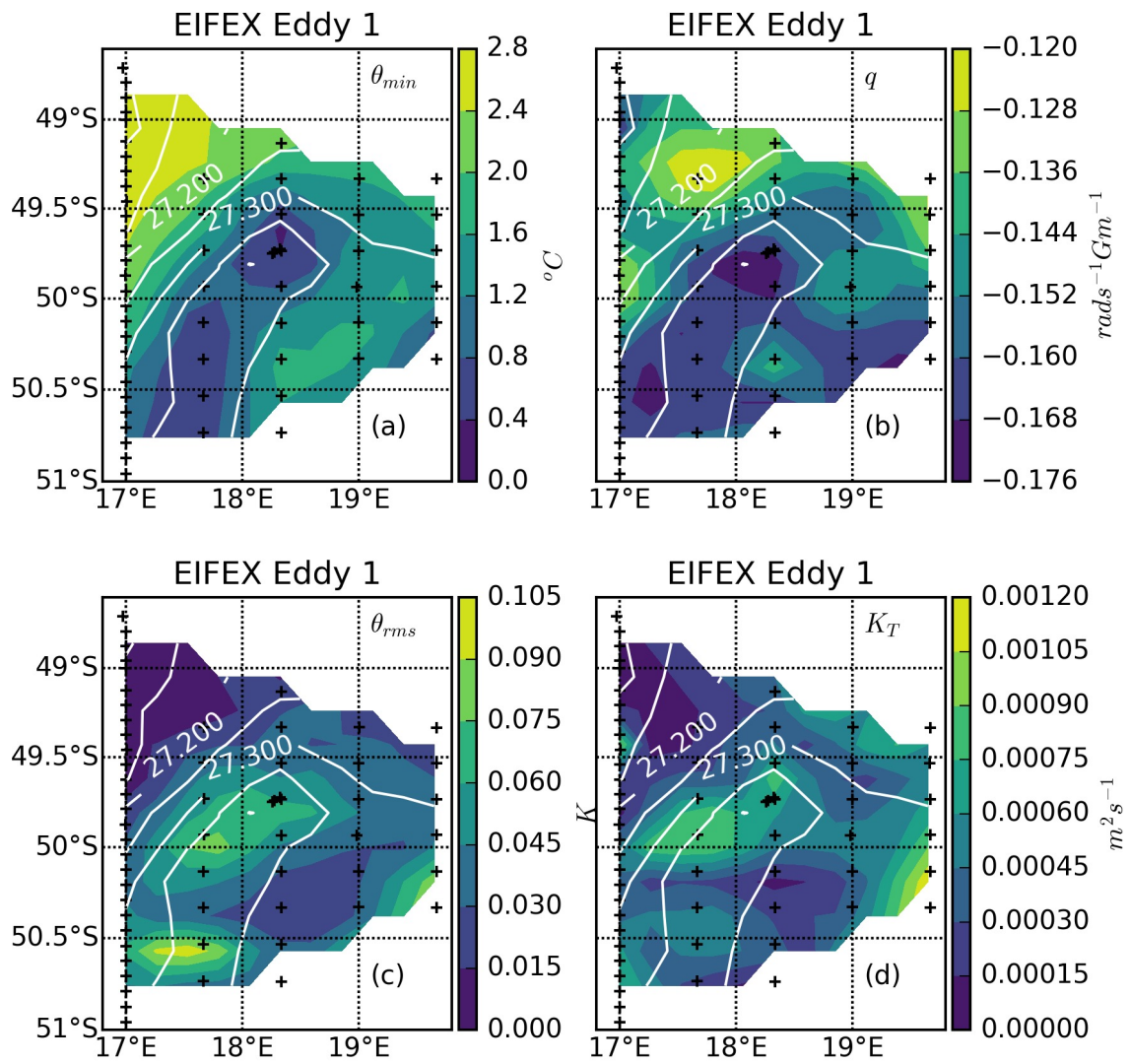


Figure 3

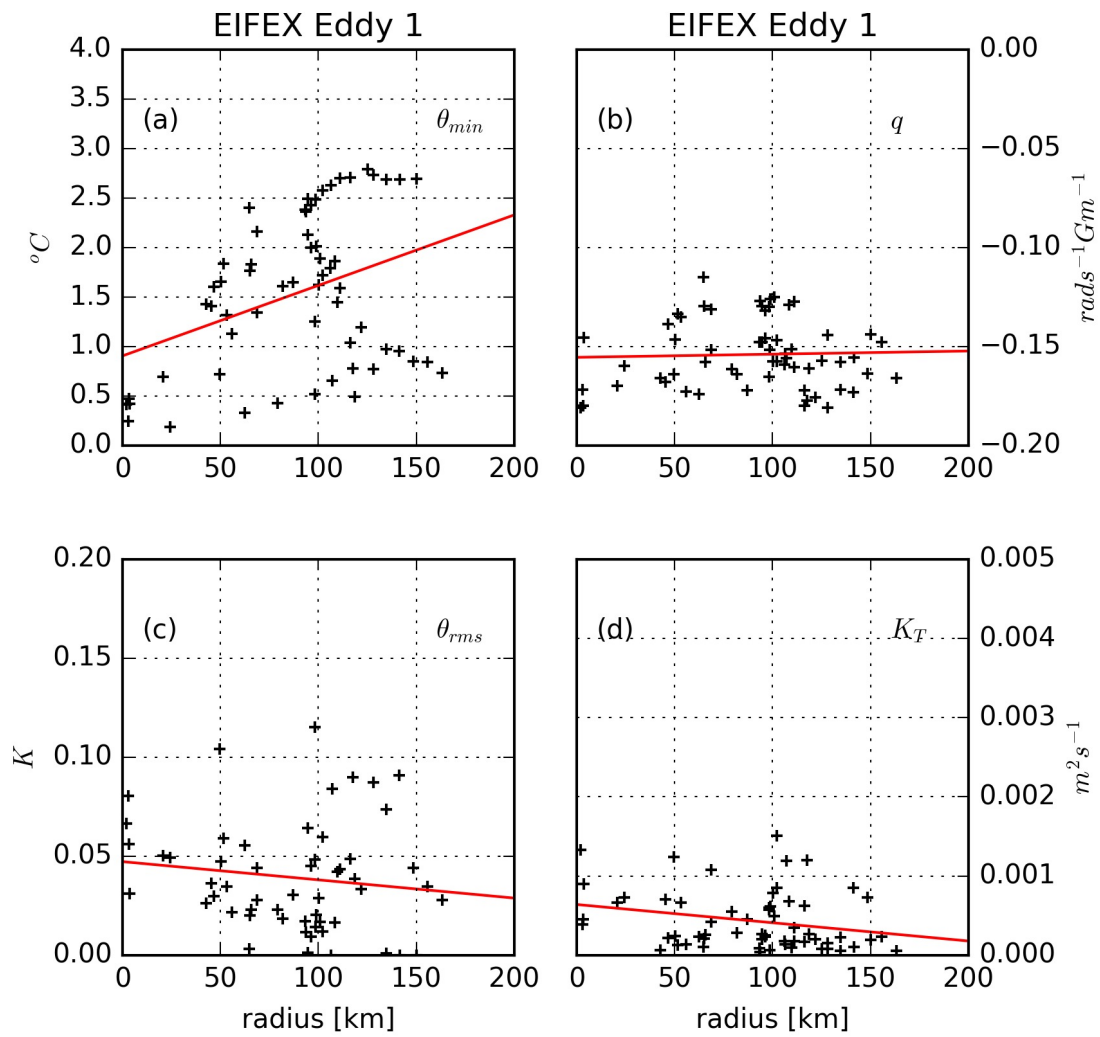


Figure 4

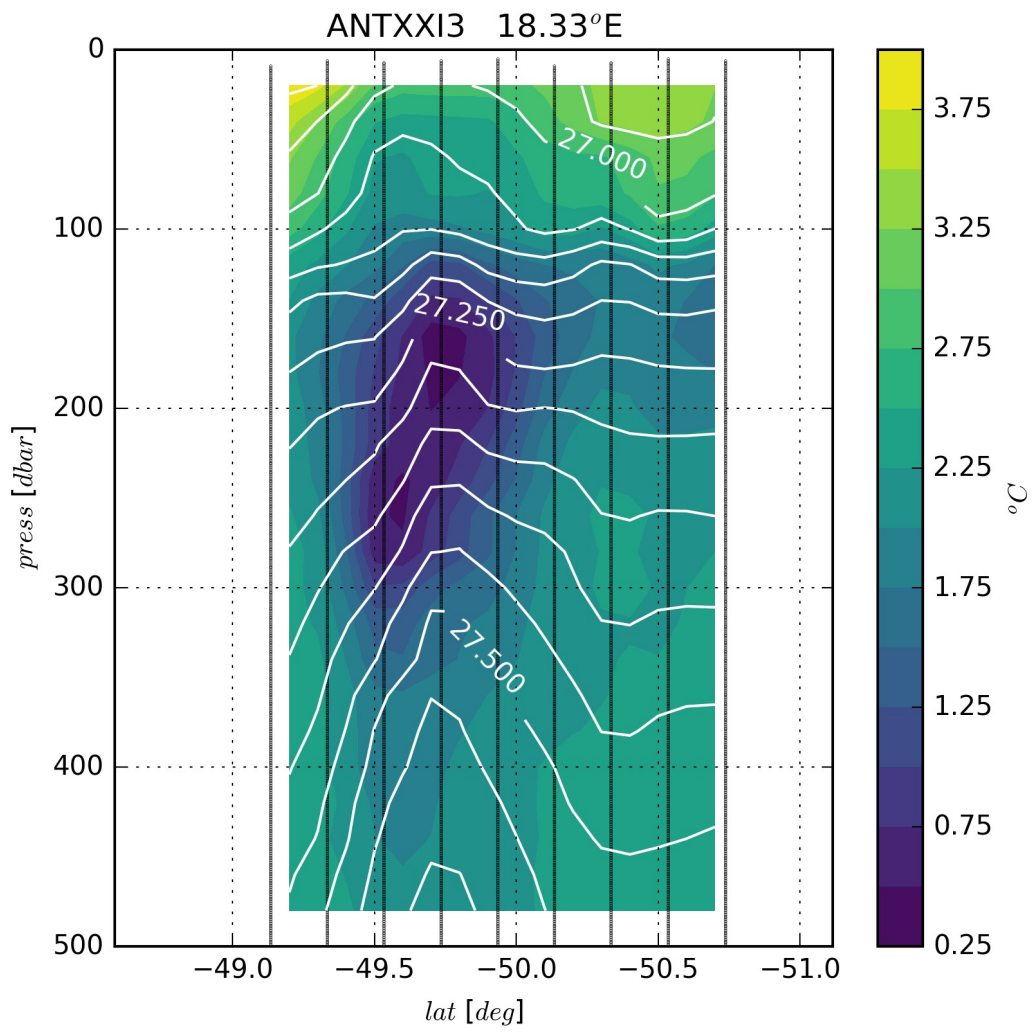


Figure 5

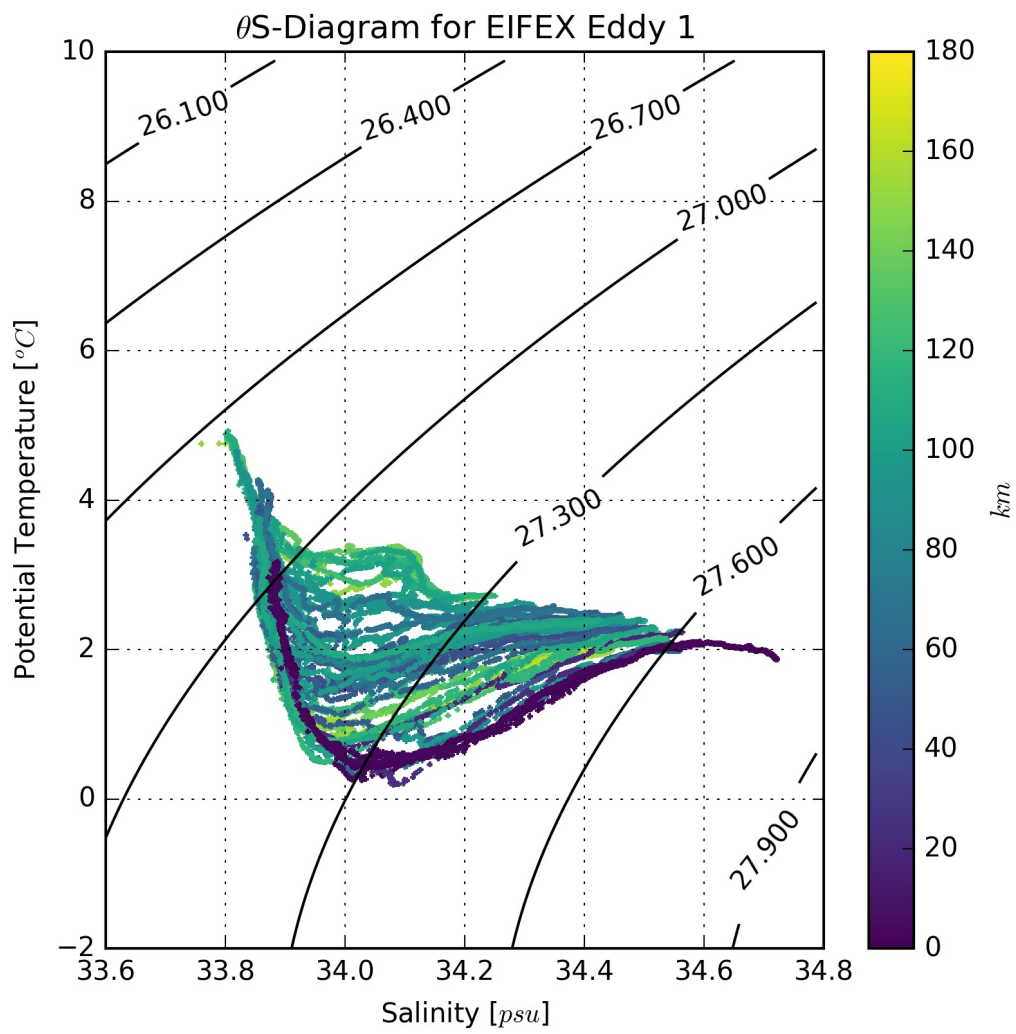


Figure 6

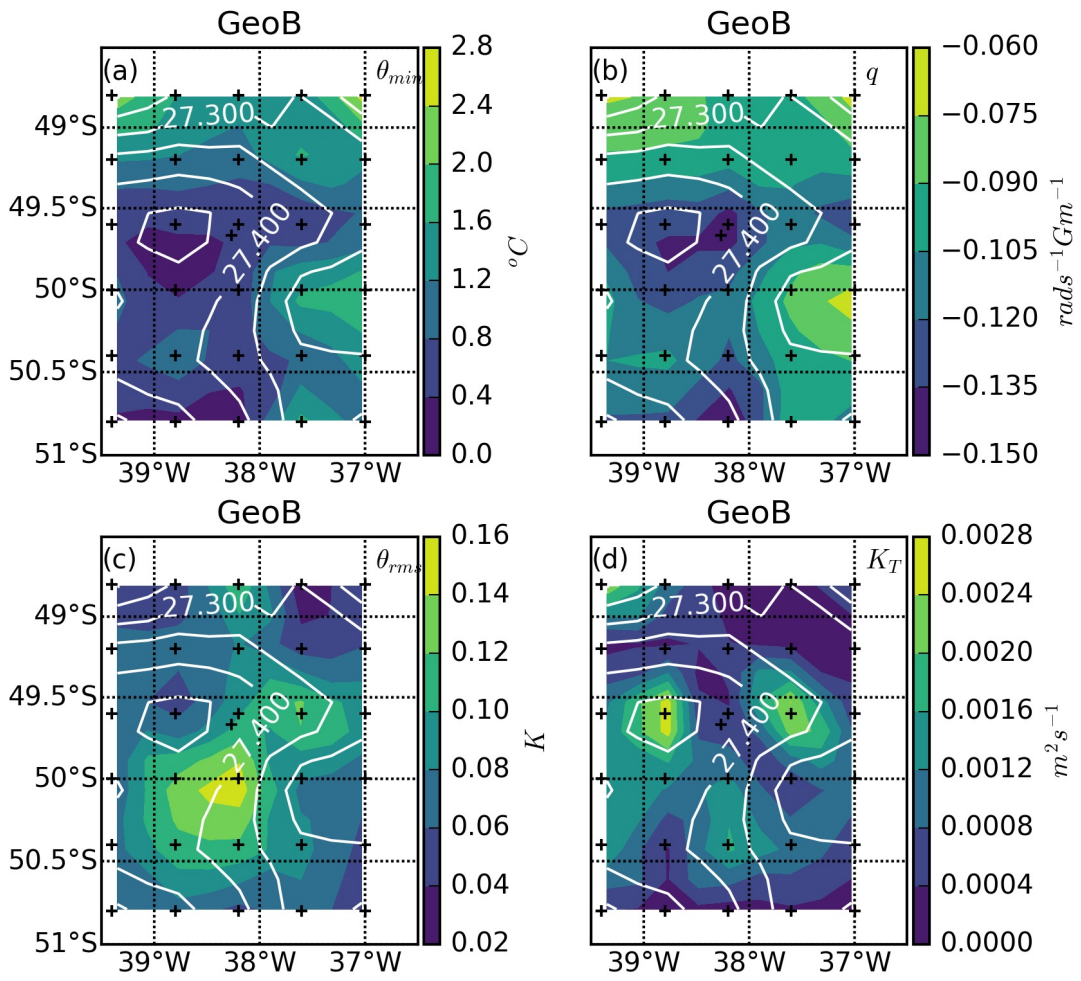


Figure 7

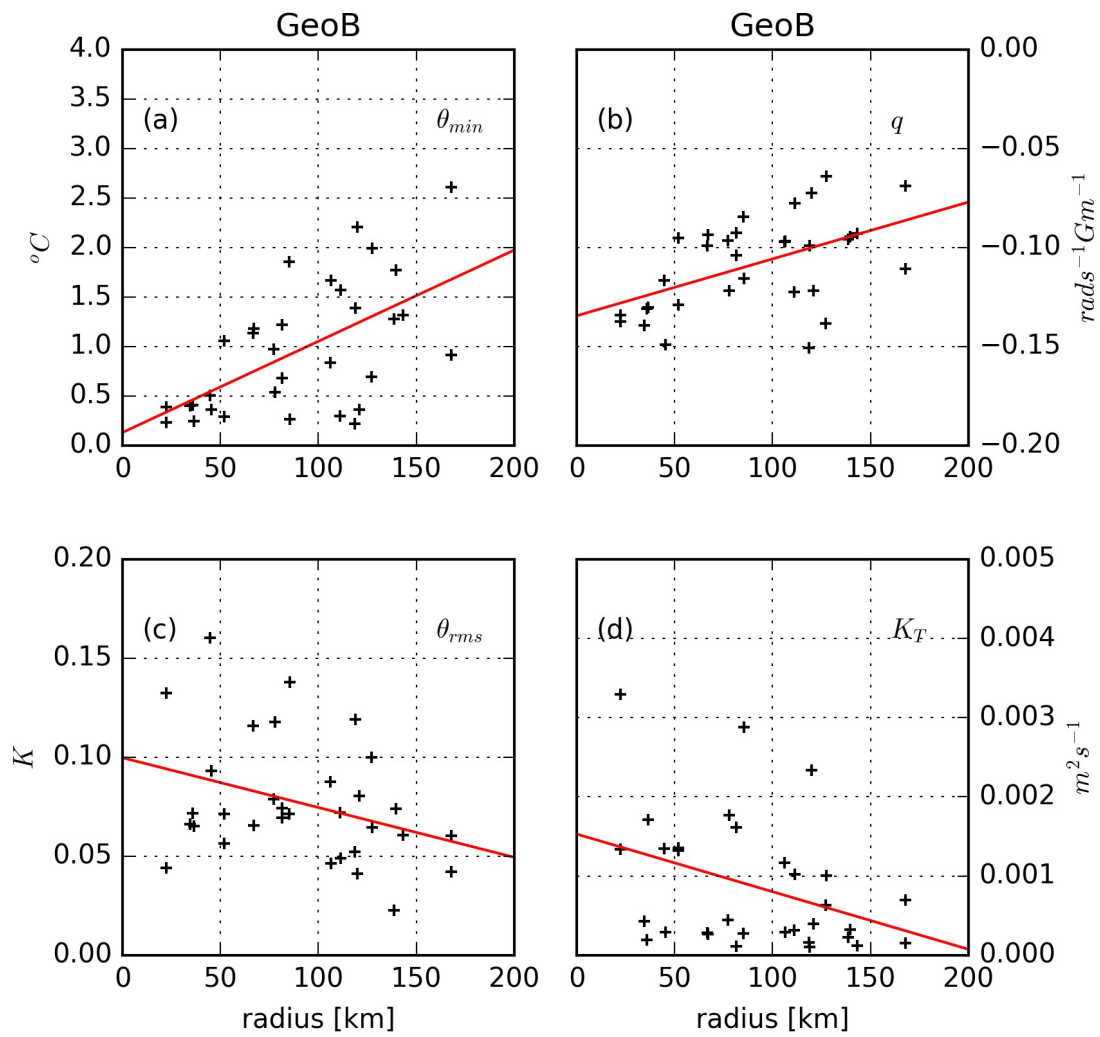


Figure 8

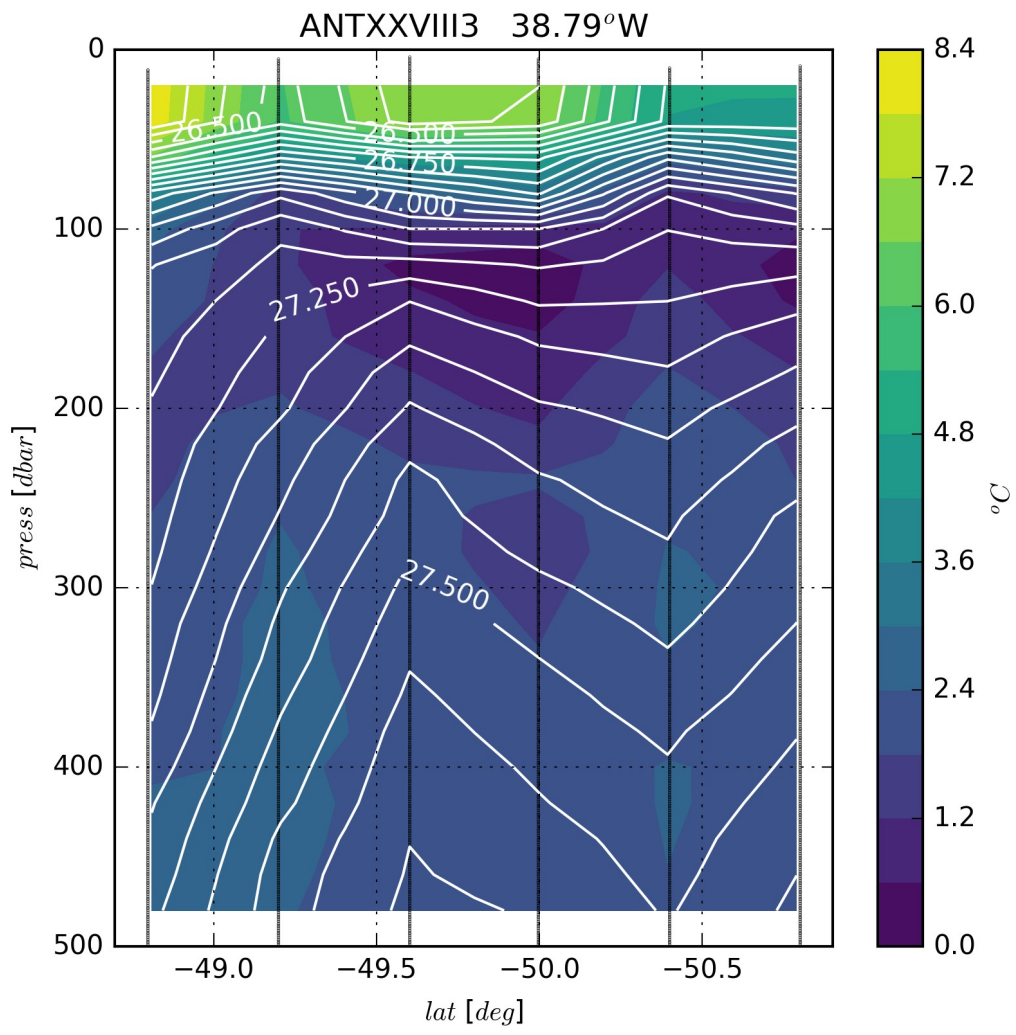


Figure 9



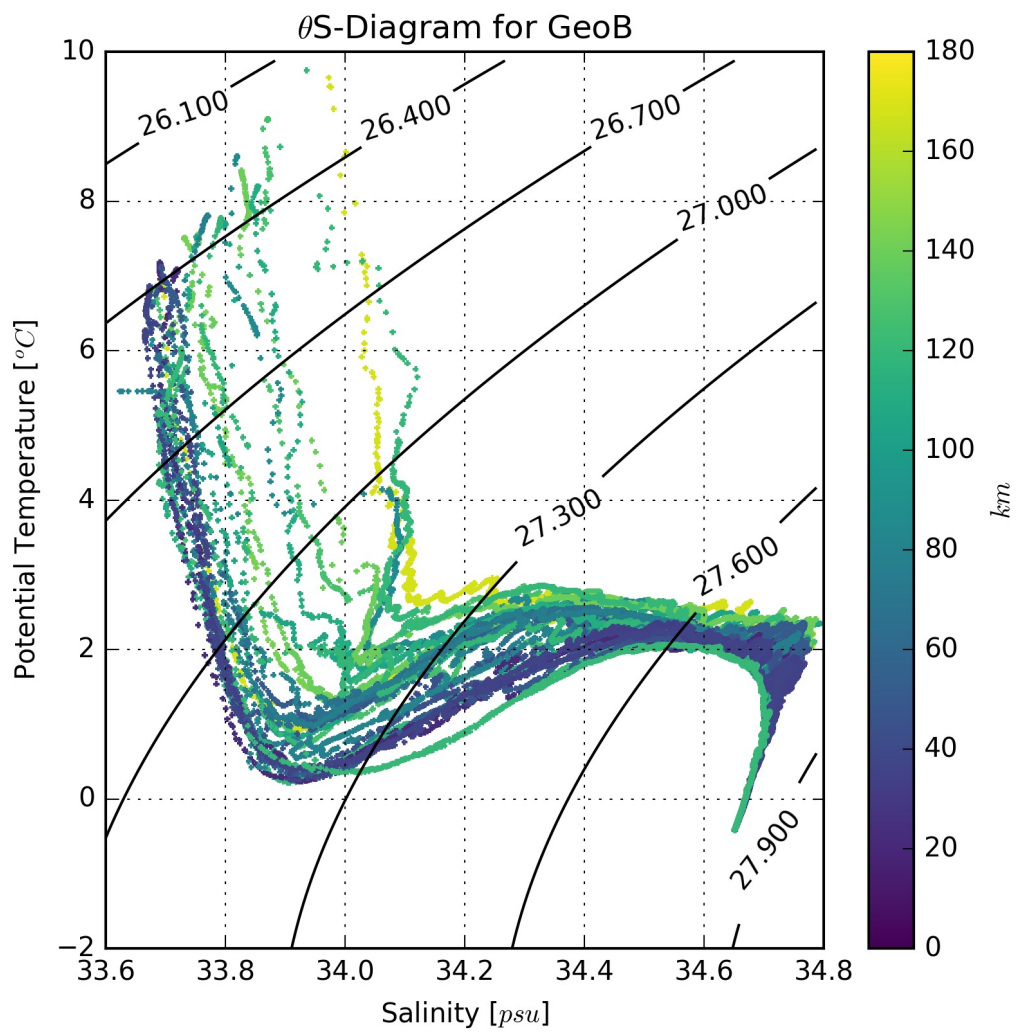


Figure 10

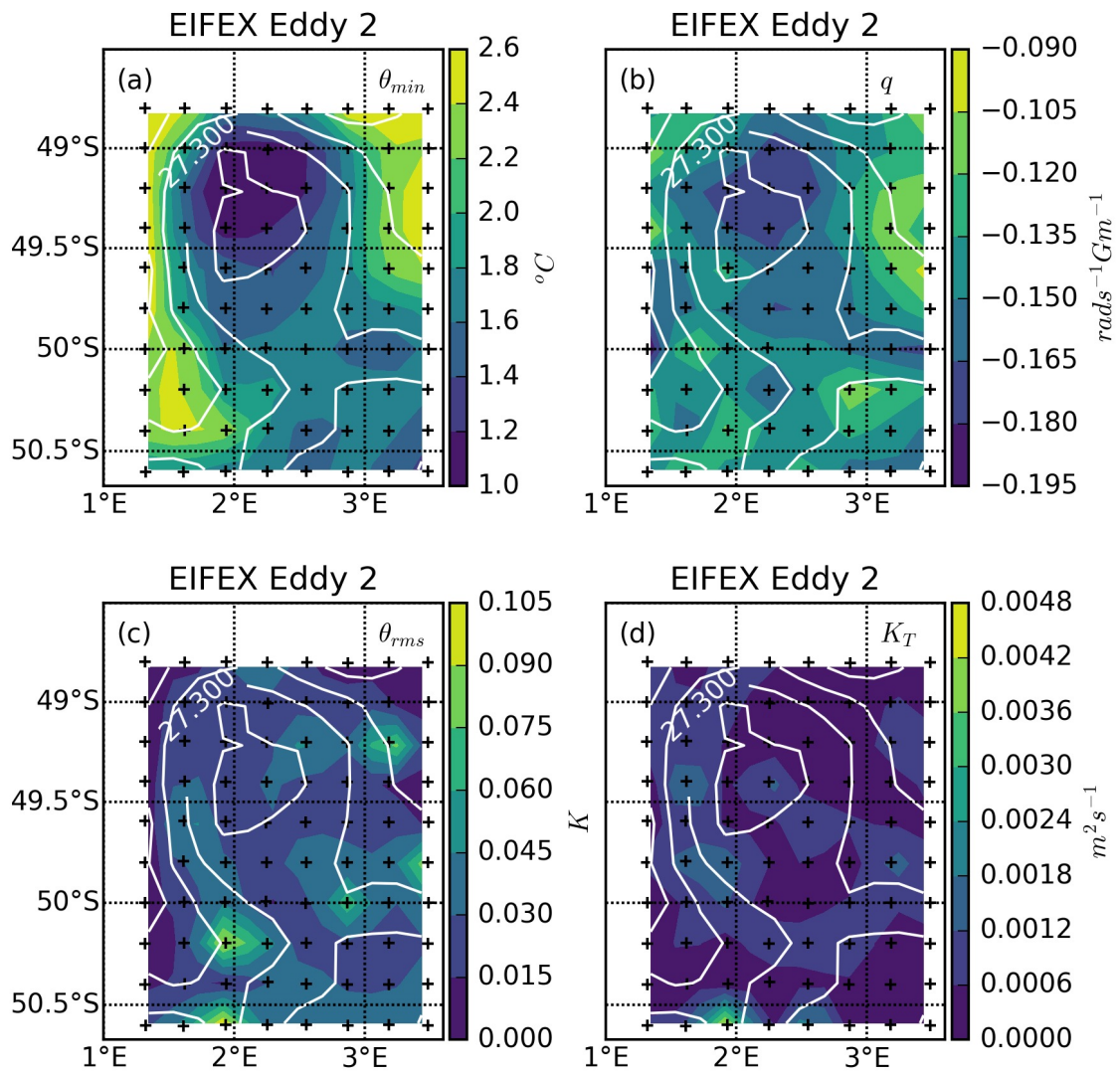


Figure 11

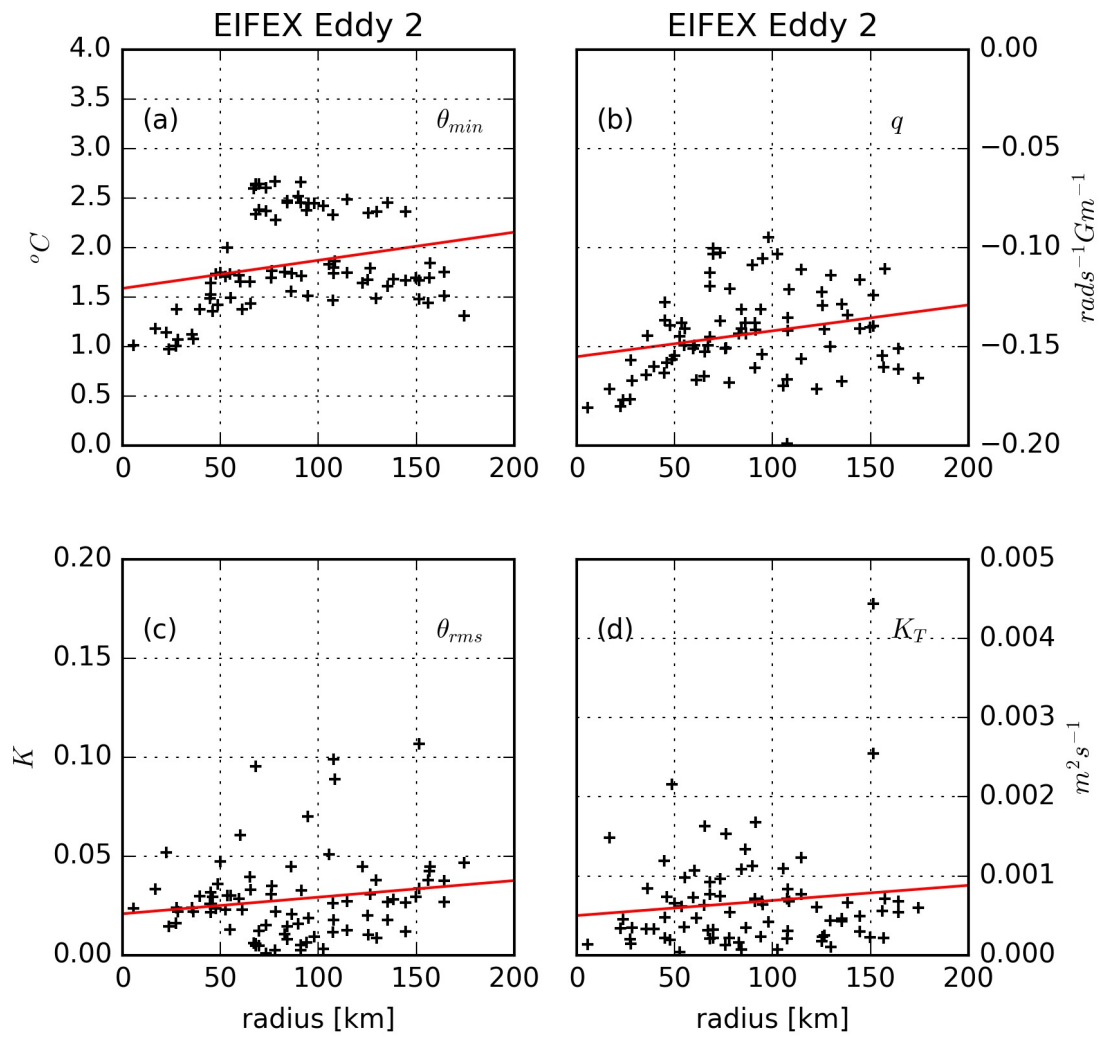


Figure 12

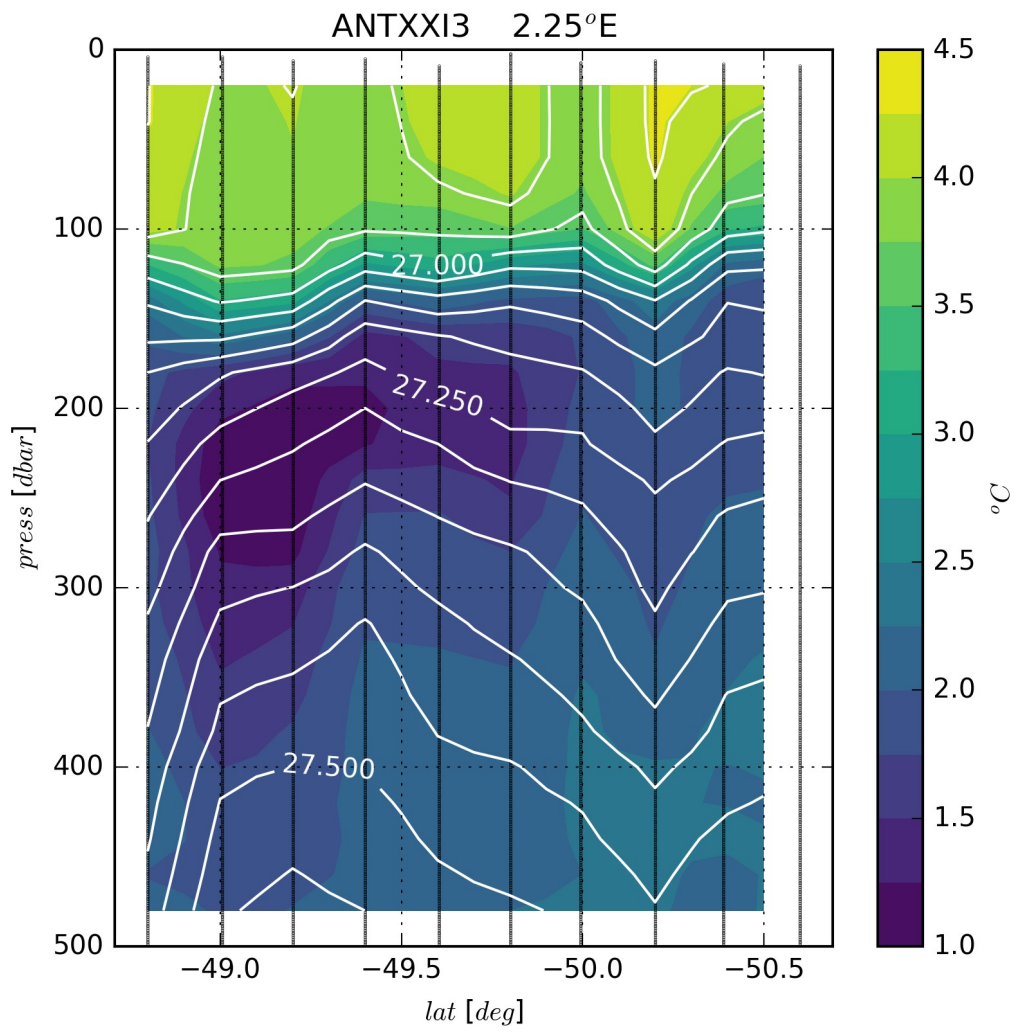


Figure 13

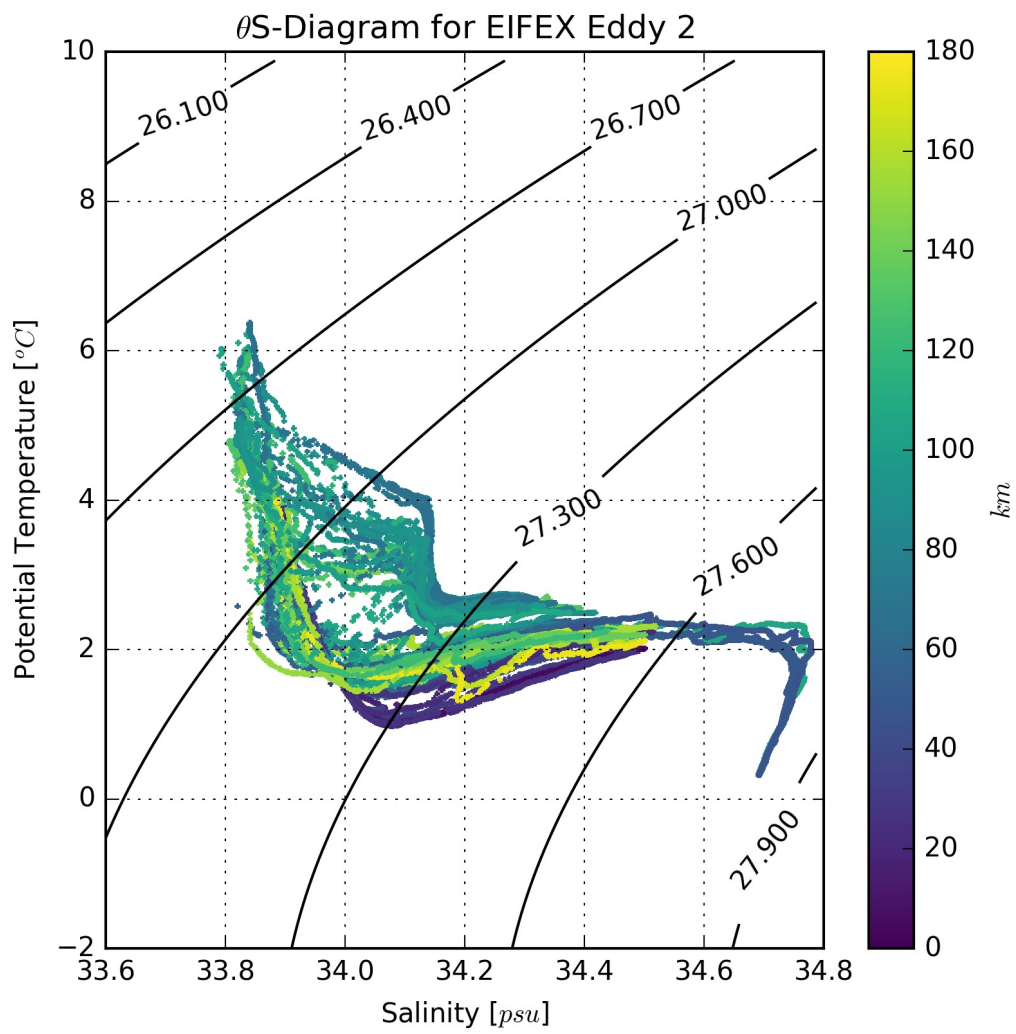


Figure 14

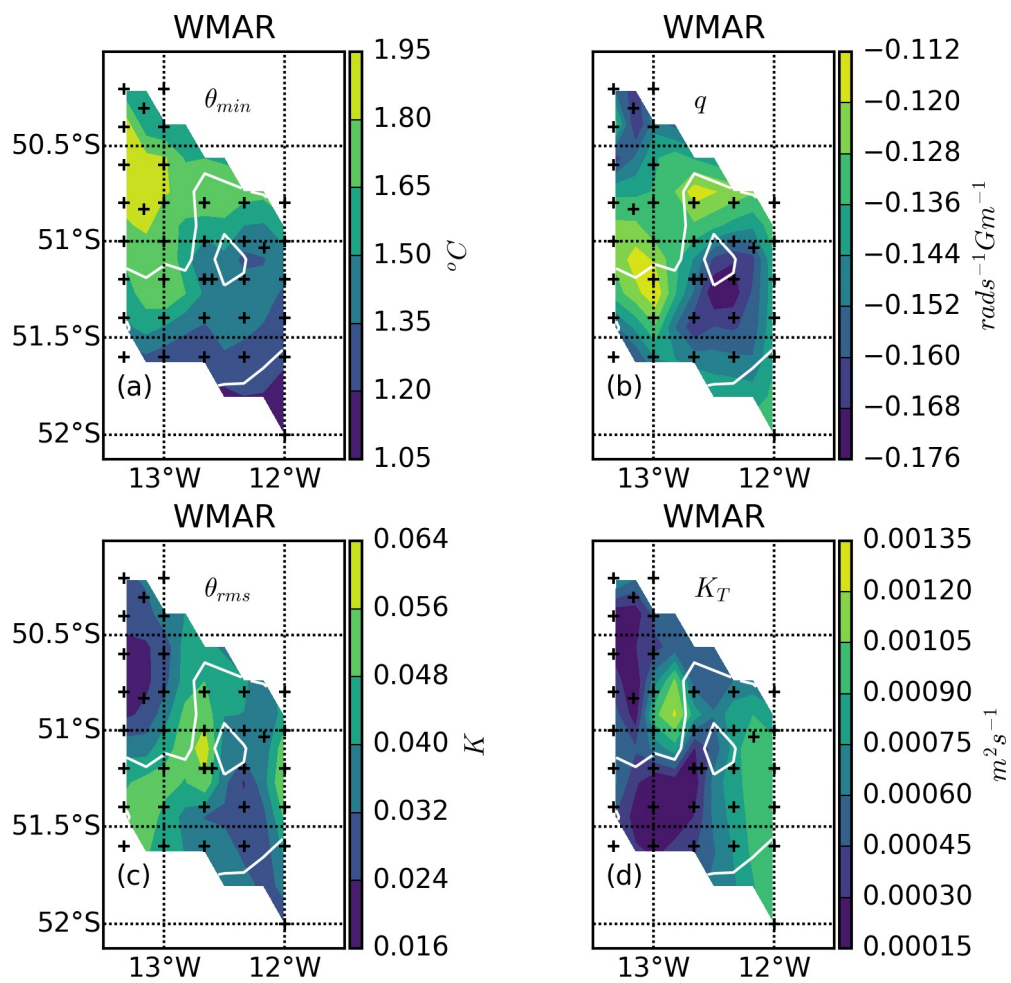


Figure 15

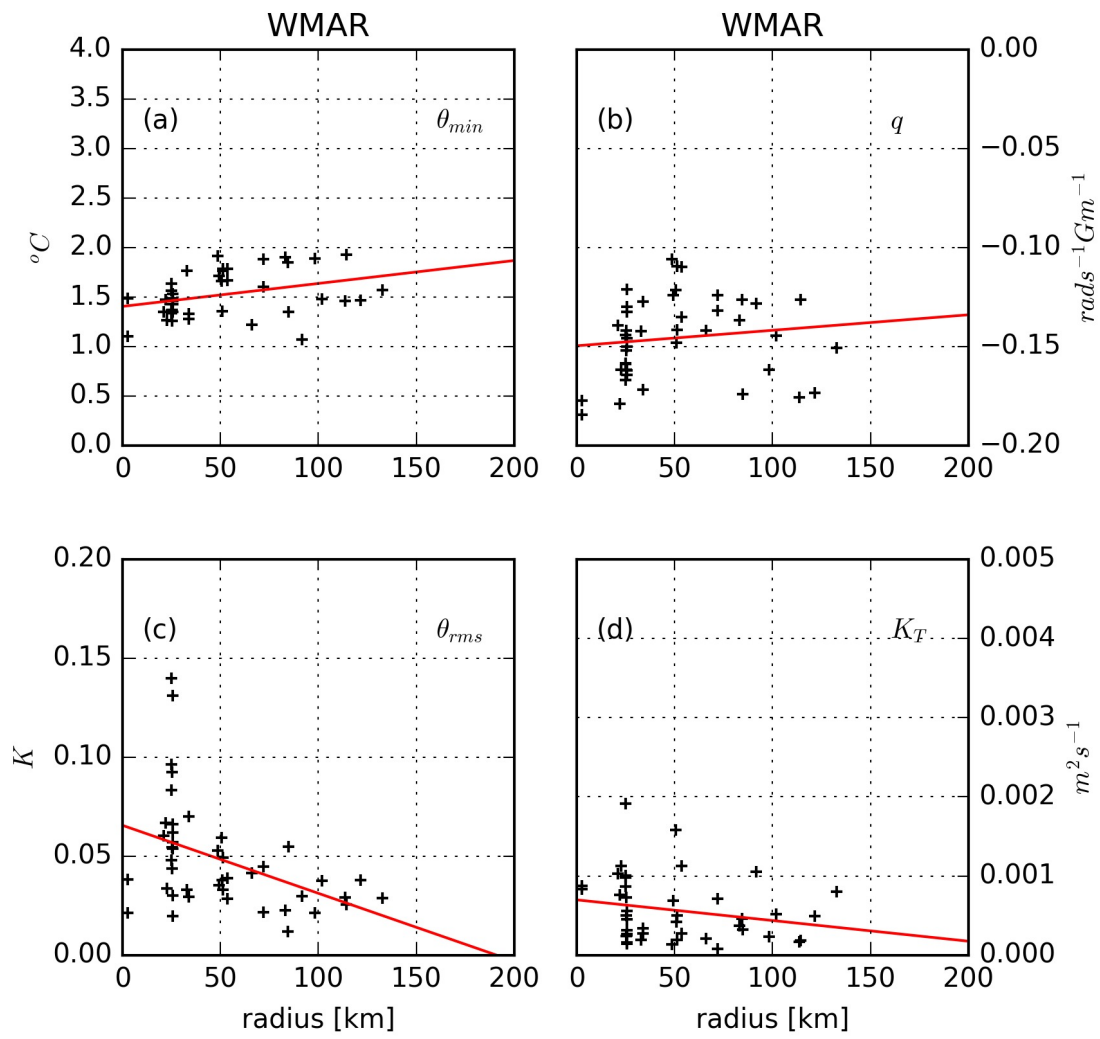


Figure 16

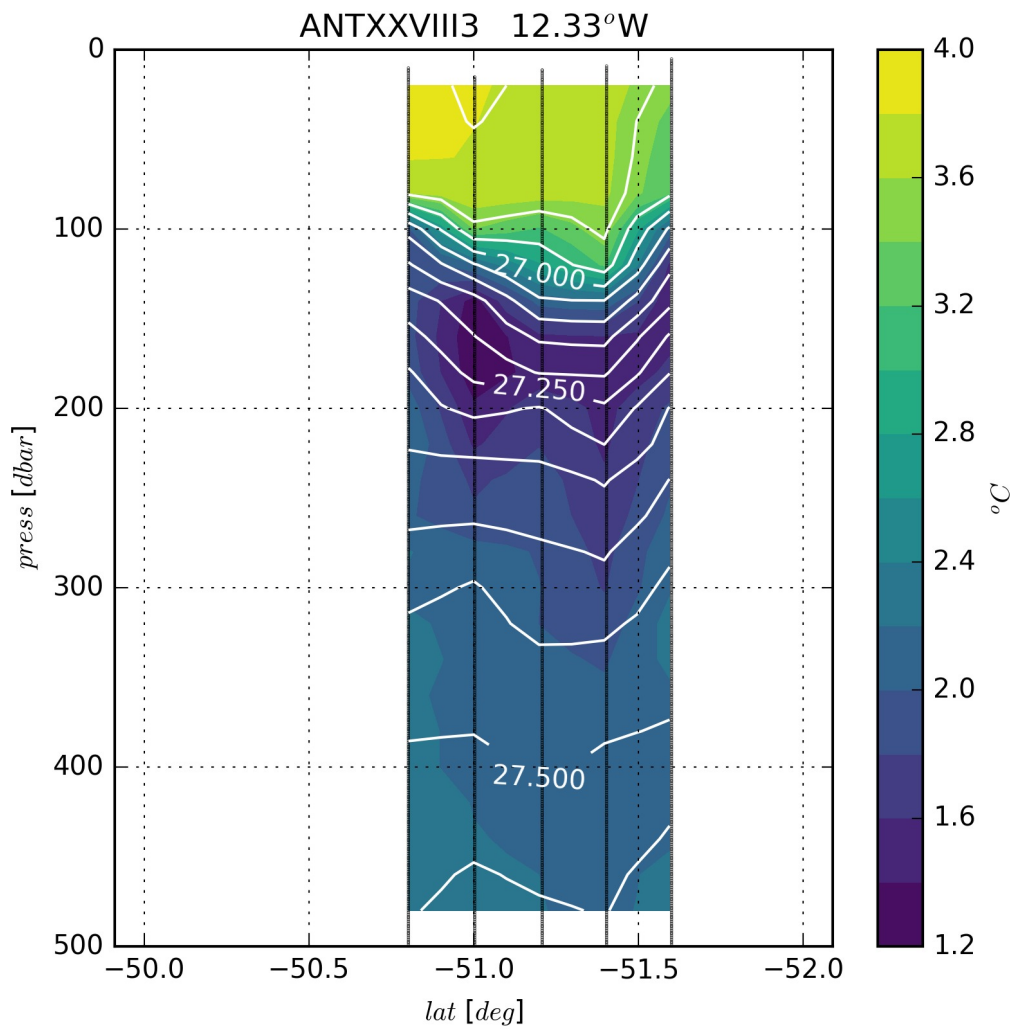


Figure 17



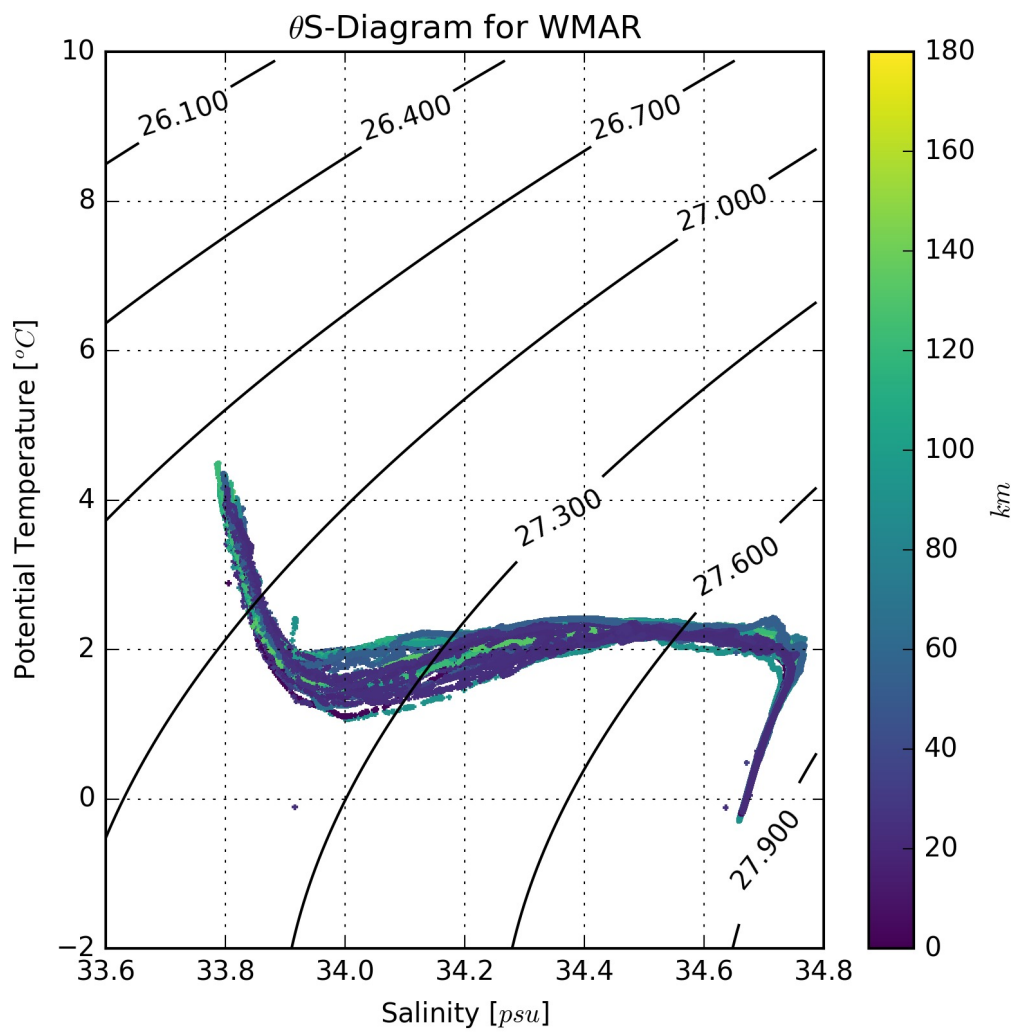


Figure 18

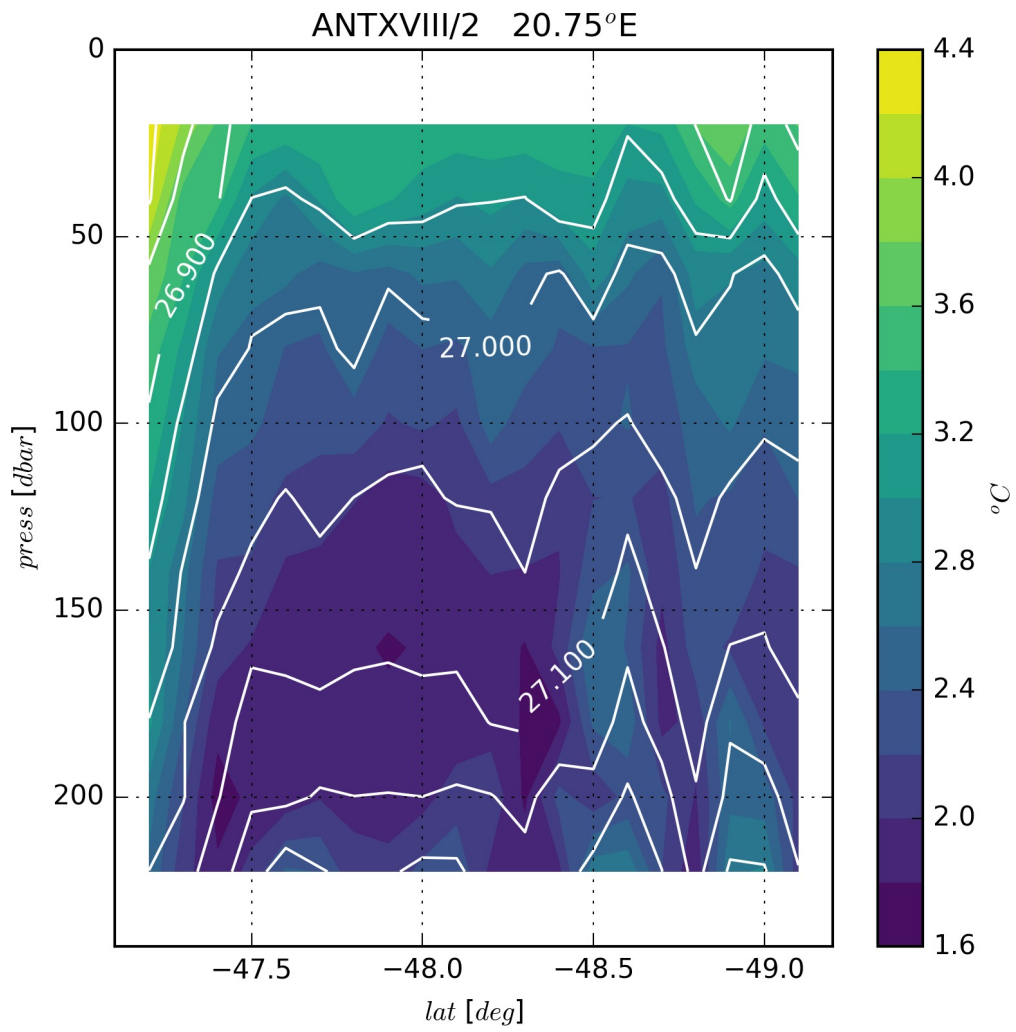


Figure 19

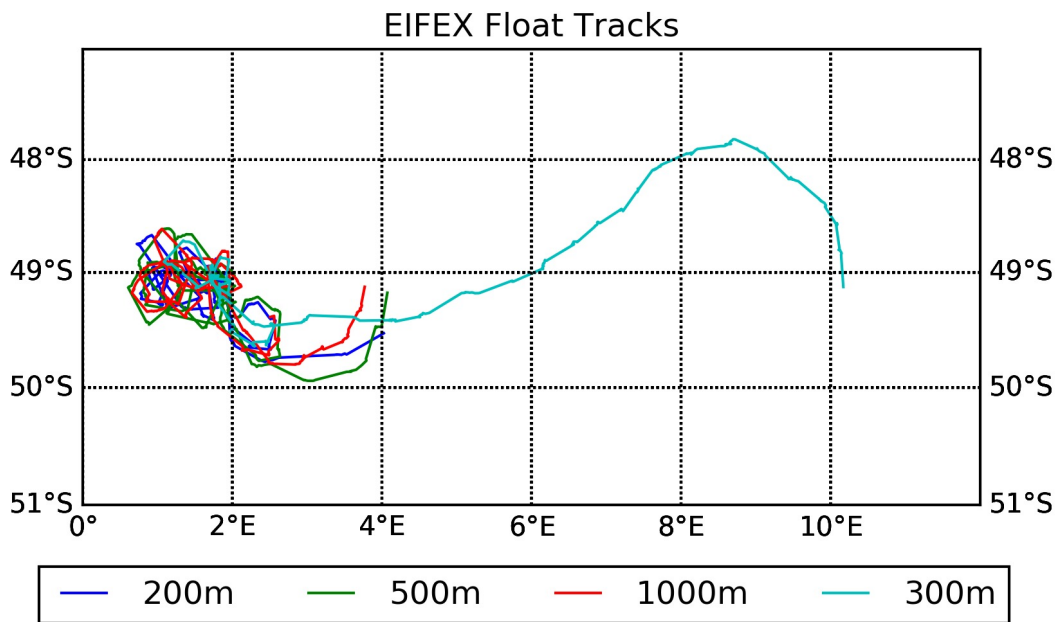


Figure 20